

DETERMINING SURFACE RESIDUAL STRESS IN STEEL SHEETS AFTER DEEP  
DRAWING AND BULGING PROCESSES

A THESIS SUBMITTED TO  
THE GRADUATE SCHOOL OF NATURAL AND APPLIED SCIENCES  
OF  
MIDDLE EAST TECHNICAL UNIVERSITY

BY

SİNEM ADIGÜZEL

IN PARTIAL FULFILLMENT OF THE REQUIREMENTS  
FOR  
THE DEGREE OF MASTER OF SCIENCE  
IN  
METALLURGICAL AND MATERIALS ENGINEERING

FEBRUARY 2011

Approval of the thesis:

**DETERMINING SURFACE RESIDUAL STRESS IN STEEL SHEETS AFTER  
DEEP DRAWING AND BULGING PROCESSES**

submitted by **SİNEM ADIGÜZEL** in partial fulfillment of the requirements for the degree of **Master of Science in Metallurgical and Materials Engineering Department, Middle East Technical University** by

Prof. Dr. Canan Özgen

Dean, Graduate School of **Natural and Applied Sciences** \_\_\_\_\_

Prof. Dr. Tayfur Öztürk

Head of Department, **Metallurgical and Materials Engineering** \_\_\_\_\_

Prof. Dr. C. Hakan Gür

Supervisor, **Metallurgical and Materials Eng. Dept., METU** \_\_\_\_\_

Assist. Prof.Dr. Celalettin Karadoğan

Co-Supervisor, **Manufacturing Eng. Dept., Atılım University** \_\_\_\_\_

**Examining Committee Members:**

Prof. Dr. Tayfur Öztürk

Metallurgical and Materials Engineering Dept., METU \_\_\_\_\_

Prof. Dr. C. Hakan Gür

Metallurgical and Materials Engineering Dept., METU \_\_\_\_\_

Prof. Dr. Rıza Gürbüz

Metallurgical and Materials Engineering Dept., METU \_\_\_\_\_

Asst. Prof. Dr. A. Caner Şimşir

Manufacturing Engineering Dept., Atılım University \_\_\_\_\_

Dr. İbrahim Çam

Central Laboratory, METU \_\_\_\_\_

**Date:**

**I hereby declare that all information in this document has been obtained and presented in accordance with academic rules and ethical conduct. I also declare that, as required by these rules and conduct, I have fully cited and referenced all material and results that are not original to this work.**

Name, Last name: Sinem ADIGÜZEL

Signature :

## ABSTRACT

### DETERMINING SURFACE RESIDUAL STRESS IN STEEL SHEETS AFTER DEEP DRAWING AND BULGING PROCESSES

Adıgüzel, Sinem

M.Sc., Department of Metallurgical and Materials Engineering

Supervisor: Prof. Dr. C. Hakan Gür

Co Supervisor: Assist. Prof. Dr. Celalettin Karadoğan

February 2011, 83 pages

The aim of this thesis is to investigate the effects of bulging and deep drawing processes on St4 cold rolled steel by simulation and experimental characterization. In the simulations, commercial software programs MSC Marc and Simufact.forming were used. The experimental studies cover metallographic investigations, hardness measurements, and residual stress measurements. Residual stress measurements were carried out by different non-destructive characterization methods; X-ray diffraction and Magnetic Barkhausen Noise. The experimental and simulation results were correlated with each other.

**Keywords:** Residual Stress, Sheet Metal Forming, Finite Element Method

## ÖZ

### DERİN ÇEKME VE ŞİŞİRME İŞLEMLERİNDEN SONRA ÇELİK SACLARIN YÜZEYKALINTI GERİLMELERİN BELİRLENMESİ

Adıgüzel, Sinem

Yüksek Lisans, Metalurji ve Malzeme Mühendisliği Bölümü

Tez Yöneticisi: Prof. Dr. C. Hakan Gür

Ortak Tez Yöneticisi: Yrd. Doç. Dr. Celalettin Karadoğan

Şubat 2001, 83 Sayfa

Bu tezin amacı derin çekme ve şişirme işlemlerinin soğuk haddelenmiş St4 çeliğinin üstündeki etkilerini simülasyon ve deneysel karakterizasyon yollarıyla araştırmaktır. Simulasyonlar MSC. Marc ve Simufact.forming ticari programları kullanılarak yapılmıştır. Deneysel çalışmalar metalografik araştırmaları, sertlik ölçümlerini ve kalıntı gerilim ölçümlerini içerir. Kalıntı gerilim ölçümleri değişik tahribatsız karakterizasyon metoduyla yapılmıştır; X ışınları kırınım ve manyetik Barkhausen gürültü metodları. Deneysel ve simülasyon sonuçları birbirini doğrulamıştır.

**Anahtar Kelimeler:** Kalıntı Gerilme, Sac Metallerin Şekillendirilmesi, Sonlu Elamanlar Yöntemi

To my hero Battal Dođanay,

## ACKNOWLEDGEMENTS

Firstly, I would like to express my deepest gratitude and appreciation to my supervisor Prof. Dr. C. Hakan Gür who inspired, encouraged and supported me during this study.

I am very thankful to Asst. Prof. Dr. Caner Şimşir for his support, inspiration, criticism and patience throughout this study.

I would also like to thank to Dr. İbrahim Çam for his guidance and help in Magnetic Barkhausen Noise measurements.

I wish to thank to ORS Bearing Company for providing the sample for experimental study and allowing me to investigate the process in detail within my study.

I would like to thank to my colleagues in Atılım University.

I send my best wishes to my friends Kıvanç Doğan Aksungur, Göksu Gürer, Derya Erdem, and Emre Coruk for their help and interest.

My special thanks go to my colleagues and friends Burcu Tolungüç whose friendship, support and suggestions made great contributions to this work.

Greatest thanks to Ufuk Öztürk, for his invaluable support, kindness and being next to me throughout the study.

Finally, I would also like to express my special thanks to my family: my parents Güler Adıgüzel and Şaban Adıgüzel for their infinite support during my whole life, my brother Necdet Adıgüzel for being joy of my life. I always need your interest.

# TABLE OF CONTENTS

<b>ABSTRACT</b> .....	<b>iv</b>
<b>ÖZ</b> .....	<b>v</b>
<b>ACKNOWLEDGEMENT</b> .....	<b>vi</b>
<b>TABLE OF CONTENTS</b> .....	<b>viii</b>
<b>LIST OF TABLE</b> .....	<b>xi</b>
<b>LIST OF FIGURES</b> .....	<b>xii</b>

## CHAPTERS

<b>1.INTRODUCTION</b> .....	<b>1</b>
1.1 General .....	1
1.2 Aim of the Work .....	3
<b>2.THEORY</b> .....	<b>4</b>
2.1 Sheet Metal Forming.....	4
2.1.1 Introduction... ..	4
2.1.2 Deep Drawing.....	4
2.1.3Bulging.....	10

2.2 Residual Stress.....	12
2.2.1 Measurement Techniques.....	14
2.2.2 X-ray Diffraction.....	16
2.2.3 Magnetic Barkhausen Noise.....	20
<b>3.LITERATURE SURVEY .....</b>	<b>24</b>
<b>4.EXPERIMENTAL PROCEDURE .....</b>	<b>29</b>
4.1 Material.....	29
4.2 Tensile Test.....	31
4.3 Compression Test.....	33
4.4 Hydraulic Bulge Test.....	33
4.5 Nakazima Test .....	38
4.6 Residual Stress Measurements by X-Ray Diffraction Method.....	41
4.7 Residual Stress Measurements by Magnetic Barkhausen Method.....	46
4.8 Finite Element Simulations.....	47
4.8.1 MSC. Marc Mentat.....	49
4.8.2 Simufact.forming.....	49
4.9 Experimental Procedure History.....	50
<b>5.RESULTS AND DISCUSSIONS .....</b>	<b>52</b>
5.1 Mechanical Tests to Determine Input data for Simulation.....	52
5.2 Microstructural Examination.....	54
5.3 Hardness Measyrements.....	55

5.4 Measurement by Magnetic Barkhausen Noise Method.....	56
5.4.1 Rollscan Results.....	58
5.4.2 $\mu$ scan Results.....	58
5.5 Measurements by X-Ray Diffraction Method.....	64
5.6 Finite Element Simulations.....	67
5.6.1 Bulging Simulation.....	68
5.6.2 Deep Drawing Simulation.....	70
5.7 Discussion.....	72
5.7.1 Residual Stress State after Bulging.....	73
5.7.2 Residual Stress State after Deep Drawing.....	74
5.7.3 Dimensional Correlation.....	74
<b>6.CONCLUSION .....</b>	<b>76</b>
<b>REFERENCES .....</b>	<b>78</b>

## LIST OF TABLES

### TABLES

<b>Table 2.1</b> Effects of Industrial Operations on Residual Stresses.....	15
<b>Table 2.2</b> Residual Stress Measurement Methods.....	17
<b>Table 4.1</b> Chemical Composition.....	29
<b>Table 4.2</b> Anisotropy Coefficient of St4.....	30
<b>Table 4.3</b> Properties of Zwick/ Roell Z300E.....	32
<b>Table 4.4</b> Experimental Statistics.....	51
<b>Table 5.1</b> Simulation Parameters.....	68
<b>Table 5.2</b> Bulging Operation Dimensional Correlation.....	75
<b>Table 5.3</b> Deep Drawing Operation Dimensional Correlation.....	75

# LIST OF FIGURES

## FIGURES

<b>Figure 1.1:</b> Deep drawing operation.....	2
<b>Figure 1.2:</b> Examples of deep drawing.....	3
<b>Figure 2.1:</b> Examples of deep drawing.....	5
<b>Figure 2.2:</b> Examples of deep-drawn parts .....	5
<b>Figure 2.3:</b> Deep drawing operation and product.....	7
<b>Figure 2.4:</b> Acting forces on deep drawn part.....	8
<b>Figure 2.5:</b> Drawing ratio relations.....	10
<b>Figure 2.6:</b> Bulging geometry.....	11
<b>Figure 2.7:</b> (a) Membrane stresses on the spherical shell. (b) Distribution of membrane strains.....	11
<b>Figure 2.8:</b> Bulging operation.....	12
<b>Figure 2.9:</b> A simple representation of X-ray diffraction.....	18
<b>Figure 2.10:</b> Flux density (B) curve as a function of magnetic field intensity (H) in ferromagnetic material.....	20
<b>Figure 2.11:</b> Barkhausen Noise Levels.....	21

<b>Figure 2.12:</b> Experimental set-up of Barkhausen.....	22
<b>Figure 2.13:</b> Effect of microstructure on Barkhausen noise.....	23
<b>Figure 3.1:</b> As tensile residual stresses increase the amplitude of the Barkhausen noise bursts also increase.....	27
<b>Figure 3.2:</b> Residual stress depth profiles measured with X-ray diffraction and estimated with Barkhausen noise analysis.....	27
<b>Figure 4.1:</b> Tensile test data of St4 cold rolled steel sheet.....	30
<b>Figure 4.2:</b> Zwick/ Roell Z300E All-round Universal Testing Machine.....	31
<b>Figure 4.3:</b> Geometric parameters of hydraulic bulge test study.....	34
<b>Figure 4.4:</b> BUP 600 hydraulic press with GOM ARAMIS.....	37
<b>Figure 4.5:</b> Typical forming limit diagram.....	39
<b>Figure 4.6:</b> Nakazima test arrangement.....	39
<b>Figure 4.7:</b> Nakazima test specimen.....	40
<b>Figure 4.8:</b> Etched sample.....	40
<b>Figure 4.9:</b> Seifert XRD 3003 PTS.....	42
<b>Figure 4.10:</b> Goniometry, TSA and X-Y Stage.....	43
<b>Figure 4.11:</b> Parabola Fit method graph.....	45
<b>Figure 4.12:</b> Center of Gravity method graph.....	45

<b>Figure 4.13:</b> Stresstech Rollscan $\mu$ Scan 500-2 device Magnetic Barkhausen Noise Equipment .....	46
<b>Figure 4.14:</b> Magnetic Barkhausen noise probe.....	46
<b>Figure 4.15:</b> The Numerical Simulation Cycle.....	48
<b>Figure 4.18:</b> User interface of Simufact.forming .....	50
<b>Figure 5.1:</b> Comparison of hydraulic bulge, tension and compression test results.....	53
<b>Figure 5.2:</b> Forming limit diagram of the cold rolled St4 sheet.....	53
<b>Figure 5.3:</b> Micrographs representing the initial microstructure of St4 steel. a) 1.8mm thickness b) 1mm thickness .....	54
<b>Figure 5.4:</b> Micrographs representing the final microstructure of St4 steel. a) Bulged sample b) Deep drawn sample .....	54-55
<b>Figure 5.5:</b> Calibration curve for Magnetic Barkhausen Noise signal versus elastic tensile stress .....	57
<b>Figure 5.6:</b> Representation of measurement direction on bulged sample.....	57
<b>Figure 5.7:</b> Surface residual stresses in the unprocessed sample, determined by MBN measurements.....	58
<b>Figure 5.8:</b> The top and side views of the bulged sample. Measurements were taken from dotted points, A1, A2, A3 and TOP; there is 2 cm between the points.....	59

**Figure 5.9:** Surface magnetic Barkhausen noise values at the selected points of the bulged sample. Measurements were taken from dotted points, A1, A2, A3 and TOP; there is 1.3 cm between the points.....60

**Figure 5.10:** Surface residual stresses at the selected points of the bulged sample. Measurements were taken from dotted points, A1, A2, A3 and TOP; there is 1.3 cm between the points.....60

**Figure 5.11:** MBN frequency distribution at the selected points on the bulged sample in the circumferential direction. Measurements were taken from dotted points, A1, A2, A3 and TOP; there is 1.3 cm between the points.....61

**Figure 5.12:** MBN frequency distribution at the selected points on the bulged sample in the axial direction. Measurements were taken from dotted points, A1, A2, A3 and TOP; there is 1.3 cm between the points.....62

**Figure 5.13:** MBN fingerprint curves at the selected points on the bulged sample in the circumferential direction. Measurements were taken from dotted points, A1, A2, A3 and TOP, there is 1.3 cm between the points.....62

**Figure 5.14:** MBN fingerprint curves at the selected points on the bulged sample in the axial direction. Measurements were taken from dotted points, A1, A2, A3 and TOP; there is 1.3 cm between the points.....63

**Figure 5.15:** Hysteresis curves at the selected points on the bulged sample in circumferential direction. Measurements were taken from dotted points, A1, A2, A3 and TOP; there is 1.3 cm between the points.....63

<b>Figure 5.16:</b> Hysteresis curves at the selected points on the bulged sample in axial direction. Measurements were taken from dotted points, A1, A2, A3 and TOP; there is 1.3 cm between the points.....	64
<b>Figure 5.17:</b> Deep Drawing stages and the final sample.....	64
<b>Figure 5.18:</b> XRD method measurement directions on deep drawn sample.....	65
<b>Figure 5.19:</b> Repeatability measurements in the central and axial directions by Center of Gravity method.....	66
<b>Figure 5.20:</b> Surface residual stresses on the deep drawn sample, in the axial and circumferential directions.....	66
<b>Figure 5.21:</b> X-ray diffraction peaks. a) Compressive residual stress state diffraction peak. b) Tensile residual stress state diffraction peak.....	67
<b>Figure 5.22:</b> 2-Theta vs. $\sin^2$ (Psi) peak from measurements.....	67
<b>Figure 5.23:</b> Tensile residual stress distributions in circumferential direction.....	69
<b>Figure 5.24:</b> Tensile residual stress distributions in axial direction.....	69
<b>Figure 5.25:</b> Residual stress level near clamp region.....	70
<b>Figure 5.26:</b> Tensile residual stress distributions in circumferential direction.....	71
<b>Figure 5.27:</b> Compressive residual stress distributions in axial direction.....	71
<b>Figure 5.28:</b> Simulation results: Residual stress distributions along the sample width in axial and circumferential directions.....	72
<b>Figure 5.29:</b> Comparison of residual stresses obtained by simulation and MBN measurements.....	73

**Figure 5.30:** Comparison of simulation (FEM) and X-ray diffraction measurement results in axial and circumferential directions.....74

# CHAPTER 1

## INTRODUCTION

### 1.1 General

Sheet metal is one of the important forms used in metal forming processes. Forming and shaping operations can be done easily and many objects used in industry made by sheet metals on nowadays. Thickness range of the sheet metals is very wide and 1 mm and 1.8 mm in thickness sheet metals are used in this study.

The sheet metal deep drawing technology is one of the most significant processes in manufacturing. By definition, deep drawing is the metal forming process used for shaping sheets into cup-shaped articles [1]. Process is shown in Figure 1.1.

Deep drawing has been categorized into two parts; *conventional* and *unconventional* deep drawing. The main advantage of any unconventional deep drawing process is to amplify the formability limits of the process. For instance, hydromechanical deep drawing is a unconventional type of deep drawing operation. [2].

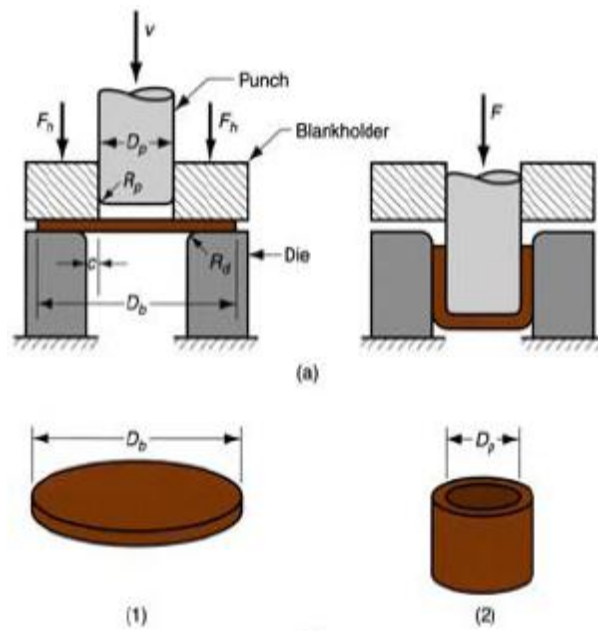


**Figure 1.1:** Deep drawing operation [3]

Production of deep drawn sheet metal includes different variables; geometric features, dimensions and used material properties. Each individual variable should be checked and planned carefully to decide best manufacturing method and parameters.. In Figure 1.2 some deep drawn parts can be seen [4].

In addition to deep drawing operation information, the residual stress phenomena should be known for obtaining logical expressions. Residual stresses are caused by different reasons; inhomogeneous plastic deformation, inhomogeneous thermal gradient and phase transformations. It can be divided into three groups, submicroscopic when the enlargement of the volume is smaller than the grain size, microscopic residual stresses when the extension is the size of the grains and in macroscopic residual stresses, when the enlargement of the volume is large compared to the grain size [5].



**Figure 1.2:** Examples of deep drawing [4]

## 1.2 Aim of the Work

There has been a huge development in simulation technology since last 20 years. The main goal of this technology is optimization of the manufacturing methods or material properties. It reduces the manufacturing time and eliminates possible problems before process starts. One can access any commercial Finite Element program for making necessary simulations. These programs are severely used for sheet metal forming simulations.

The aim of this thesis is to investigate the effects of bulging and deep drawing on St4 cold rolled steel by simulation and experimental characterization. In the simulations, commercial software programs MSC Marc and SIMUFACT.forming were used. The experimental studies cover metallographic investigations, hardness measurements, and residual stress measurements. Residual stress measurements were carried out by two non- destructive characterization methods; X-ray diffraction and Magnetic Barkhausen Noise. The experimental and simulation results were correlated with each other.

## **CHAPTER 2**

### **THEORY**

#### **2.1 Sheet Metal Forming**

##### **2.1.1 Introduction**

Today very large volume of sheet metal rolls can be produced by rolling mills with very low costs. Sheet metal form is very popular because of any metal can be produced in this form. Moreover, these sheets can be used in secondary processes for automotive industry, domestic products, aerospace technology, food and drink cans and a wide range of other applications. They have a high elastic modulus and high yield strength. As a results of these mechanical properties the products can be stiff and have a good strength-to-weight ratio, because of these good properties are very favorable in industry.

Common sheet metal forming operations are listed below. Details of these can be found in reference [6].

##### **2.1.2 Deep Drawing**

Sheet metal is formed by stretching in deep drawing operations. Punch pushes the blank downward and forces it into a die cavity in the shape of the desired part. The tensile forces resulting from punch motion carried out to the blank bring about it to plastically deform into a cup-shaped part.

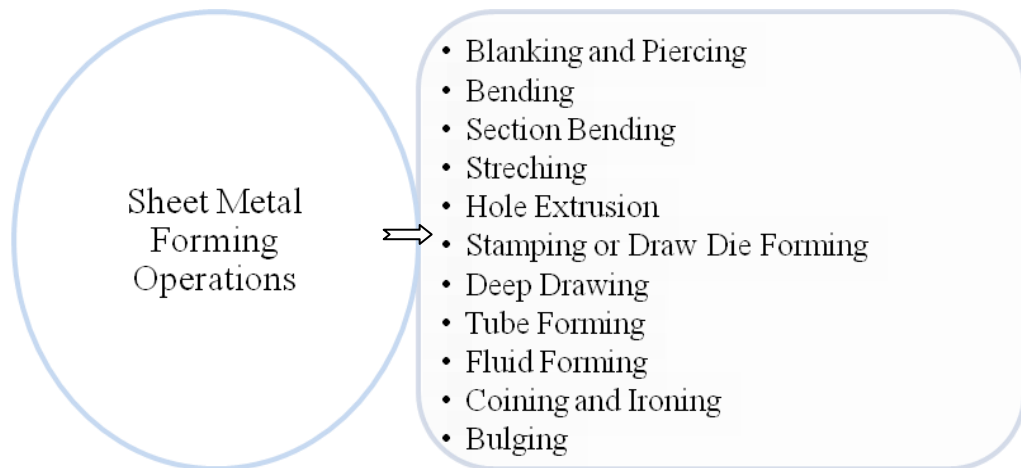


**Figure 2.1** Examples of deep drawing [4]

Deep drawn parts are categorized by a depth equal to more than half of the diameter of the part. The most common ones are cylindrical and rectangular parts. Ductile metals like aluminum, mild steel and brass can be deep drawn easily. Refrigerator bodies, bearings, drinking cans, bathroom sinks are some examples of deep drawing products

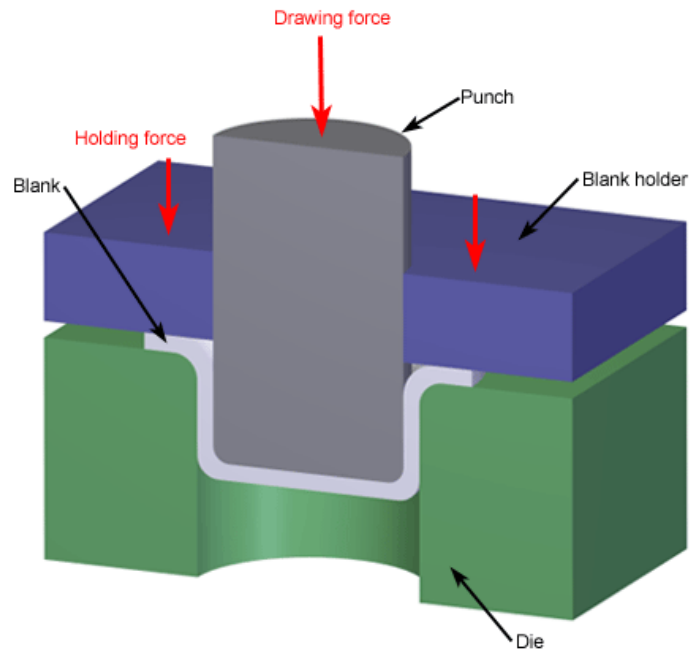


**Figure2.2:** Examples of deep-drawn parts [7]

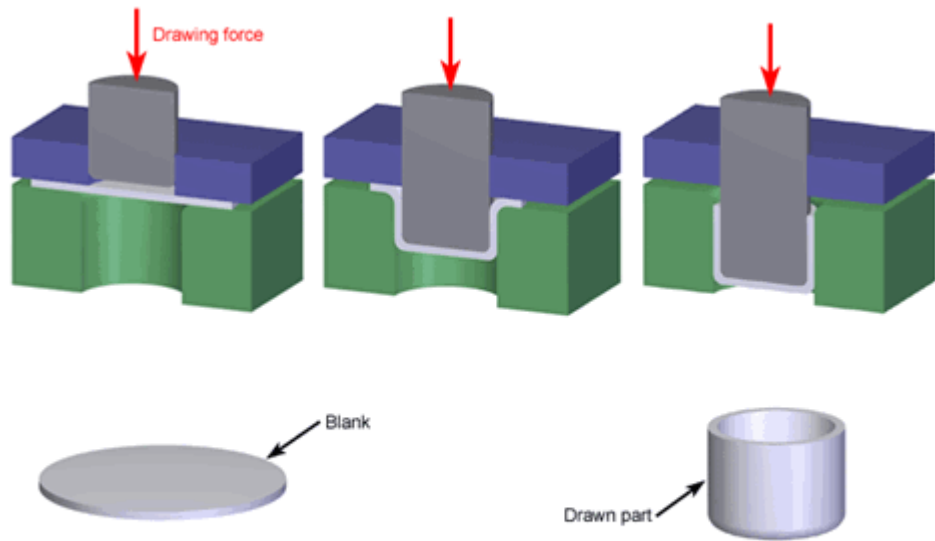
In deep drawing operations there should be a blank, blank holder, punch, and die. The blank's shape typically a circle or rectangle, which is will be formed into the

part. The blank is pressed down by the blank holder over the die, which has a cavity in the external shape of the part. Then, punch moves downward into the blank and draws or stretches the material into the die cavity. Hydraulically powered punch is usually used to apply enough force to the blank. Both the die and the punch are from tool steel or carbon steel against wear. The process of drawing part sometimes occurs in several steps, called draw reductions. In each step, a punch draws the part into a different die, stretching the part to a greater depth in each time. After a blank is completely drawn, the punch and blank holder can be raised and the part ejected from the die. If any flange is formed, it will be trimmed off. In figure the deep drawing operation and deep drawing sequence is showed [7].

The sheet metal is exposed to radial compression forces  $F_R$  and tangential tension forces  $F_T$  (Figure 2.4). In the radial direction, the sheet is compressed and stretched in the tangential direction. As a result, the blank thickens at the flange region after deep drawing operation. However, there is thinning at the bottom. There is a high liability of bulging in the flange region due to tension forces. If the tension forces at the flange region pass a critical limit, the wrinkling occurs. Therefore, the blank holding forces, and draw beads are utilized to control the flowing of the material into the die cavity for overcoming effects of tension forces. Because of there is a strongly non-homogeneous deformation throughout the part, residual stresses arise. There will be tensile residual stresses on outside and compressive residual stresses on the inside of the part in axial direction. These stresses are maximum near the top of the wall where there was little net tension because of bending. One should be careful about these residual stresses (deep-drawn parts), because they may cause problems during machining or heat treatment operations. The problems may be minor like changing geometry or may be major like fracture.



Copyright © 2009 CustomPartNet



Copyright © 2009 CustomPartNet

**Figure 2.3:** Deep drawing operation and product [7]

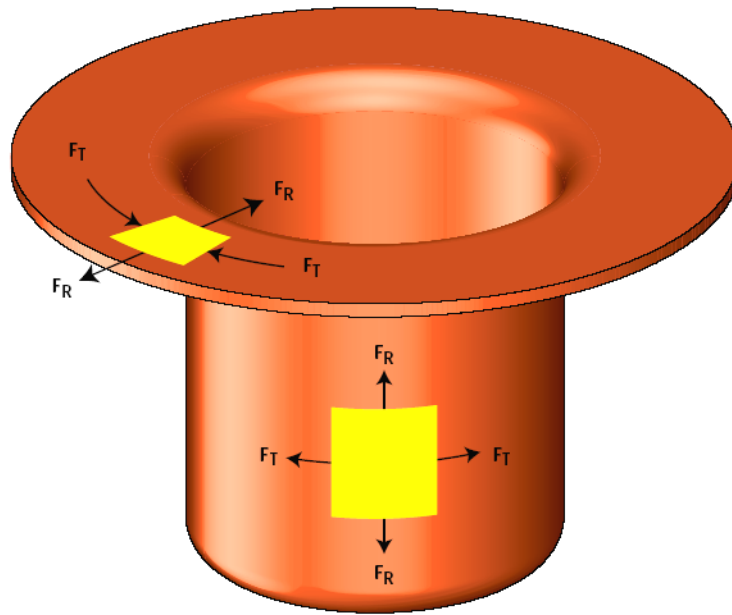


**Figure 2.4:** Acting forces on deep drawn part [8]

Generally, by the draw depth is increased, the deformation amount and the deformation resistance are also increased. The sheet is most drastically stretched in the corner of the draw punch corresponding to the tip of the drawn cup. Failure usually occurs at this region of the blank. Moreover, in some metals, splitting of the walls by stress-corrosion cracking is occurred due to unbalanced forces [8].

Deep Drawing operations have several parameters; material properties, machine parameters such as tool and die geometry, work piece geometry and working conditions. These parameters fix the sheet material behavior in mechanical forming process [9].

Limiting Drawing Ratio (LDR) may be the most important parameters in deep drawing operation. LDR is the ratio of the initial blank form's diameter to the diameter of the drawn part

$$\beta = \frac{D}{d} \quad (2.1)$$

Where  $D$  is the initial sheet metal's diameter and  $d$  is the diameter of the punch. The draw ratio  $\beta$  is a critical numerical value for cylindrical deep drawing parts in calculating the required number of drawing steps.

The maximum  $\beta$  depends on the properties of the sheet material used and some other factors like friction. If the friction between the drawn part and the punch is low, then in the base part failure will occur. If the friction between the blank and the punch exceeds the critical limits, then the failure zone moves to the body part. In order to ensure a secure production process, it is preferable to select a draw ratio value that is rather equal or less than the critical limit value.

As a rough estimate, the first drawing can be calculated as having a maximum ratio of  $\beta = 2$ . To achieve  $\beta > 2$  several drawings should be carried out and it must be noted that  $\beta$ , because of work hardening, can only reach a level of 1.3 in the next drawing step. When the part is annealed before the next drawing operation, a  $\beta$  of 1.7 can be assumed.

With several drawing steps, the total draw ratio becomes a product of the individual draw ratios [8]:

$$\beta_{total} = \beta_1 \cdot \beta_2 \cdot \beta_3 \dots \cdot \beta_n \quad (2.2)$$

LDR is reduced when blank-holder force  $B$  and strain-hardening are greater, because the rate of increase in the average flow stress in the flange will be greater than the strengthening of the cup wall. LDR is increased by better lubrication reducing the friction coefficient  $\mu$ , a more ample die corner radius, increasing the bend ratio  $\rho/t$  and anisotropy characterized by  $R > 1$ . [6]

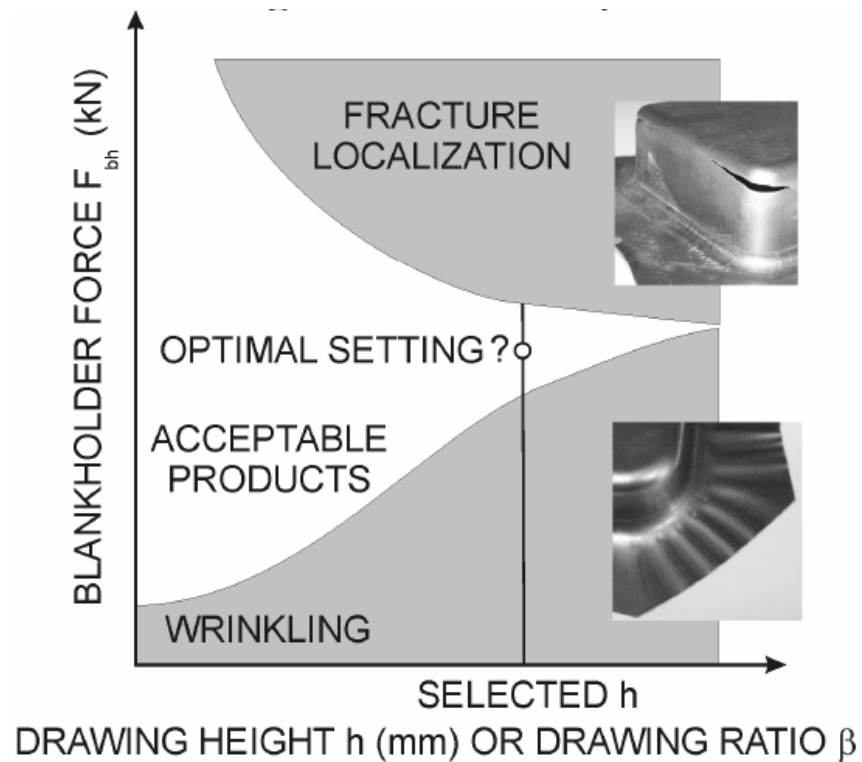


**Figure 2.5:** Drawing ratio relations [10]

### 2.1.3 Bulging

Sheet may be bulged to an approximately spherical shape by fluid pressure as shown in Figure 2.6. Although this process is used to obtain mechanical properties in sheet, it also used for forming operations. As shown below, the blank is clamped rigidly around the edge.

The membrane stresses are illustrated in Figure 2.7(a). As the edge of the disc is clamped, the circumferential strain at the edge must be zero, as shown in Figure 2.7 (b). As indicated, the membrane strains become equal at the pole where  $r = 0$ .

The most important reason for using this technique is that quite large strains can be obtained before failure even in materials having very little strain-hardening. The membrane strain at failure in biaxial stress is greater than the strain at necking in the tensile test [11].

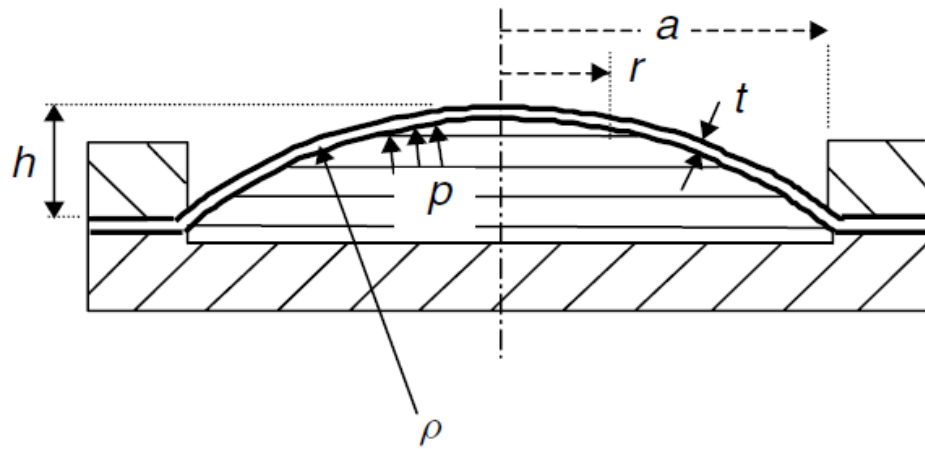


**Figure 2.6:** Bulging geometry [11]

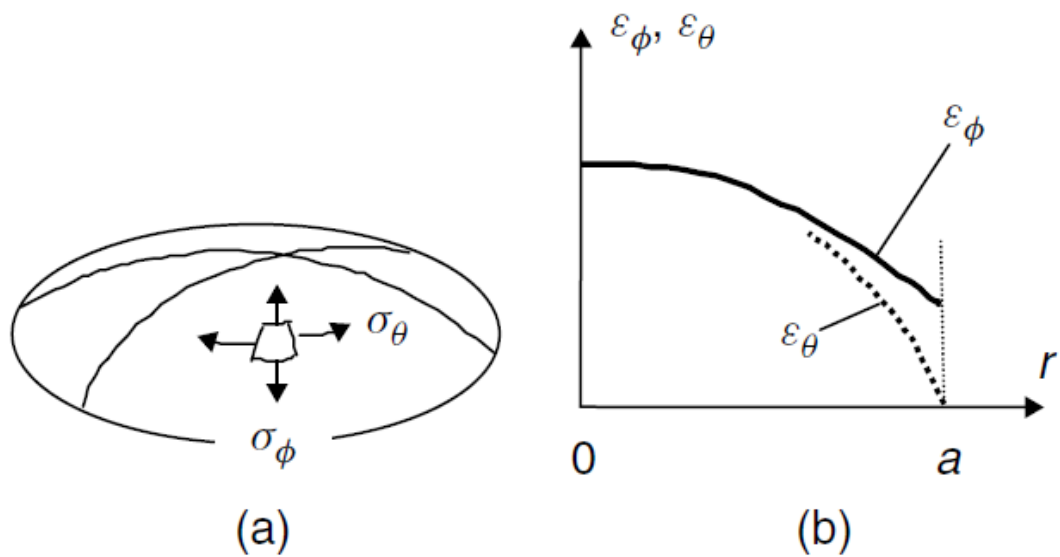


**Figure 2.7:** (a) Membrane stresses on the spherical shell. (b) Distribution of membrane strains [11]

Figure 2.8 shows an example of conventional bulging machine and produced bulging sample.

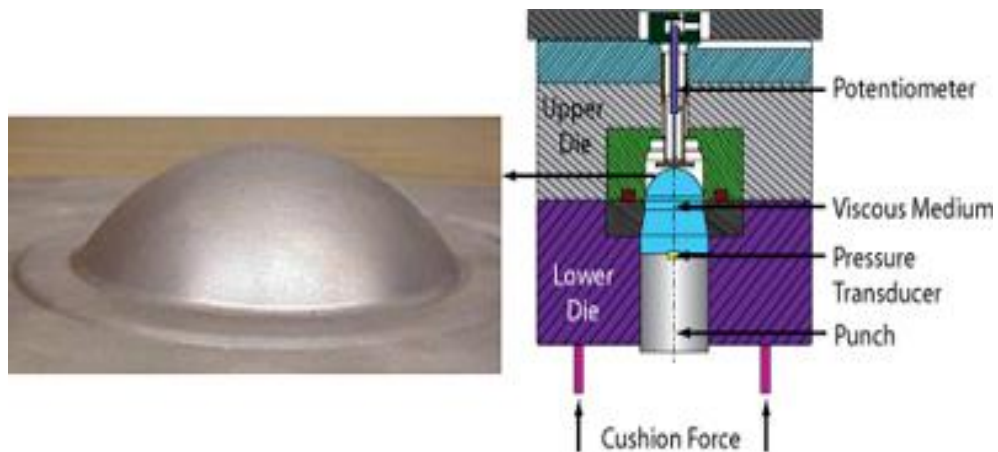


**Figure 2.8:** Bulging operation [7]

## 2.2 Residual Stress

Residual stresses are defined as unknown stresses which are left in a product, by a manufacture or assembly method, after all external forces are removed. Residual stresses can be caused by different reasons such as thermal, chemical and plastically induced misfits between different regions of a component. The state of the residual stress depends on both the material properties of the sample and the applied processes.

Residual stresses are usually known as affect the service life of the products negatively. In many cases unexpected failures are occurred due to presence of residual stresses such as fatigue, stress-corrosion cracking or brittle fracture. Although this is a general phenomenon, compressive residual stresses improve the fatigue life of the component as in shot peening operation.

Residual stresses are characterized according to their length over the stresses balance. Type I stresses equilibrate over macroscopic dimensions. These macroscopic stresses are seen across the particular finite length in a component.

Type II stresses equilibrate over grain dimensions (3–10 x grain size). Type III stresses exist over atomic dimensions [12], [13]

Macroscopic residual stresses are occurred due to:

- Non-homogeneous plastic flow under during forming operation (shot peening, auto-fretting, roller burnishing, shock laser treatment),
- Non-homogeneous plastic deformation during non-uniform heat treatment (ordinary quenching, moulding of plastics),
- Structural deformation from metalworking (heat treatment),
- Non-homogeneous chemical or crystallographic order,
- Surface treatments (nickel-plating, chrome-plating, PVD and CVD coating),
- Having different expansion coefficients and mechanical incompatibility of different components of the composites (composites with a metallic and organic matrix, ceramic coatings).

Type II residual stresses are occurred due to:

- Each crystal or grain has non- homogeneous and anisotropic characteristic in a polycrystalline material.

Type III residual stresses are occurred due to:

- Crystalline defects like vacancies, interstitial or substitution atoms, dislocations, stacking defects, twin crystals and grain boundaries.

Mechanical engineers and designers interest into Type I residual stresses. Therefore, macro residual stress states of the samples were measured in this study. However, Type II residual stresses are also important because of the indicator of strain-hardening. It alerts against failure [13].

Table 1 shows the effects of industrial metal working or surface treatment operations on residual stresses. One can handle one or more processes listed in the table during production operations. Estimation of the residual stress for product can be found by knowing before all else the source of the stresses.

### **2.2.1 Measurement Techniques**

Knowledge of total stress state plays an important role in understanding the failure phenomena. Total stress is composed of applied stresses and residual stresses. Usually one can exactly calculate the applied stress, but the residual stress calculations cannot be very accurate. Therefore, residual stresses are found by experimentally [13].

Measuring residual stress is very important in order to explain or prevent failure of the product. For instance, some processing errors can cause devilish tensile residual stresses which can progress failure. If the residual stress state of the components can be fixed before usage, many failures will be hindered, but it must be considered that the internal residual stresses which are three-dimensional balanced in a component. This means that negative residual stresses are counter balanced by positive residual stresses [15].

There are a lot of residual stress measurement techniques. Necessary information about the methods is summarized in Table 2.

In this study X-ray diffraction and Magnetic methods were used.

**Table 2.1: Effects of Industrial Operations on Residual Stresses [14]**

<b>ORIGIN</b>	<b>MECHANICAL</b>	<b>THERMAL</b>	<b>STRUCTURAL</b>
<b>PROCESS</b>			
<b>Smelting Casting</b>	No	Temperature gradient during cooling	Change of phase
<b>Shot-peening Hammer-peening Roller- burnishing Shock Laser Treatment Bending Rolling Chasing Forging Straightening Extrusion</b>	Heterogeneous plastic deformation between the core and surface of the part	No	No
<b>Grinding Turning Milling Drilling Boring</b>	Plastic deformation due to the removal of chips	Temperature gradient due to heating during machining	Change of phase during machining if the temperature is sufficiently high
<b>Quenching without a Phase Change</b>	No	Temperature gradient	Non
<b>Surface Quenching with a Phase Change (Induction, EB, Laser, Plasma, Classical Methods)</b>	No	Temperature gradient	Change of volume due to a phase change
<b>Case-hardening Nitriding</b>	No	Thermal incompatibility	New chemical component with D V
<b>Welding</b>	Flanging	Temperature gradient	Microstructural change (HAZ)
<b>Brazing</b>	Mechanical incompatibility	Thermal incompatibility	New phase at interface
<b>Electroplating</b>	Mechanical incompatibility	Mechanical incompatibility	Composition of plating depending on bath used
<b>Hot Spraying (Plasma, Laser, Jet Kote)</b>	Mechanical incompatibility, micro-cracking	Thermal incompatibility, temperature gradient	Change of phase in plating
<b>PVD, CVD</b>	Mechanical incompatibility	Mechanical incompatibility	Change of phase
<b>Composite</b>	Mechanical incompatibility	Mechanical incompatibility	No

### **2.2.2 X-Ray Diffraction**

X-ray diffraction technique is one of the most favorite residual measurement techniques. The technique draws on the fact that when a metal is under residual stress, the produced elastic strains cause the atomic planes in the metallic crystal structure to change their spacing. This interplanar atomic spacing can be directly measured by X-ray diffraction, and from this value the total residual stress on the metal can be derived. Stress is an extrinsic property so that it depends on other things and cannot be measured by itself. Stress can be determined by measuring some intrinsic property, such as strain or force and area, and the calculation of the associated stress [17].

Since crystals are known as regular three-dimensional array arrangement for metals, most metals have polycrystalline structure (some of them have single crystal structure). When this polycrystalline metal is subjected to stress, elastic strains are produced in the crystal lattice (interatomic strain). X-ray diffraction technique can measure the interatomic spacing that is indicative of the elastic strain in the specimen. By assuming there is a proportion between the stress and strain values and knowing the elastic constants, stress values can be derived from these elastic strain values [18].

There are different measurement methods like mechanical and non linear elastic methods. However, they are limited in their applicability to residual stress determination. Mechanical methods, generally destructive, cannot be checked by repeating the measurement and limited by the nature of residual stress. Moreover, they have less spatial and depth resolution than those of X-ray diffraction.

**Table 2.2:** Residual Stress Measurement Methods [16]

Method	Penetration	Spatial Resolution	Accuracy	Comments
Hole drilling (distortion caused by stress relaxation)	~1.26 x hole diameter	50 $\mu\text{m}$ depth	$\pm 50$ MPa, disadvantage; reduced sensitivity with increasing depth	Measures in-plane type I stresses; semi-destructive
Curvature (distortion as stresses arise or relax)	0.1–0.5 of thickness	0.05 of thickness; no lateral resolution	minimum measurable curvature	Unless used incrementally, stress field not uniquely determined; measures in-plane type I stresses
XRD (atomic strain gauge)	<50 mm (Al); <5 mm (Ti); <1 mm (with layer removal)	1 mm laterally; 20 $\mu\text{m}$ depth	$\pm 20$ MPa, limited by non-linearities in $\sin^2\psi$ or surface condition	Non-destructive only as a surface technique; sensitive to surface preparation; peak shifts: types I, <II>; peak widths: type II, III
Hard X-rays (atomic strain gauge)	150 – 50 mm (Al)	20 $\mu\text{m}$ lateral to incident beam; 1 mm parallel to beam	$\pm 10 \times 10^{-6}$ strain, limited by grain sampling statistics	Small gauge volume leads to spotty powder patterns; peak shifts: type I, <II>, II; peak widths: types II, III
Neutrons (atomic strain gauge)	200 mm (Al); 25 mm (Fe); 4 mm (Ti)	500 $\mu\text{m}$	$\pm 50 \times 10^{-6}$ strain, limited by counting statistics and reliability of stress free references	Access difficulties; low data acquisition rate; costly; peak shifts: type I, <II> (widths rather broad)
Ultrasonics (stress related changes in elastic wave velocity)	>10 cm	5 mm	10%	Microstructure sensitive; types I, II, III
Magnetic (variations in magnetic domains with stress)	10 mm	1 mm	10%	Microstructure sensitive; for magnetic materials only; types I, II, III
Raman	< 1 $\mu\text{m}$	< 1 $\mu\text{m}$ approx.	$\Delta\lambda \approx 0.1 \text{ cm}^{-1} \equiv 50 \text{ MPa}$	Types I, II

All nonlinear elastic methods cause error from preferred orientation, cold work, temperature, and grain size. In these methods calibration samples are needed, and it should be stress-free. Nowadays, these are not used for determination of residual stress state. Furthermore, they have lower spatial and depth resolutions than those of X-ray diffraction.

One should be measure elastic strain in the crystal lattice at least twice, moreover the orientation with respect to sample surface should be known. Therefore, XRD residual stress measurement method is suitable for the materials that are crystalline, relatively fine grained, and produces diffraction for any (known) orientation of the sample surface. XRD method's samples may be metallic or ceramic as long as a diffraction peak of suitable intensity and free of interference from neighboring peaks can be produced in the high back-reflection region with the radiations available. X-ray diffraction residual stress measurement is unique in all types of residual stresses can be determined nondestructively and nearly gives the most accurate results [18].

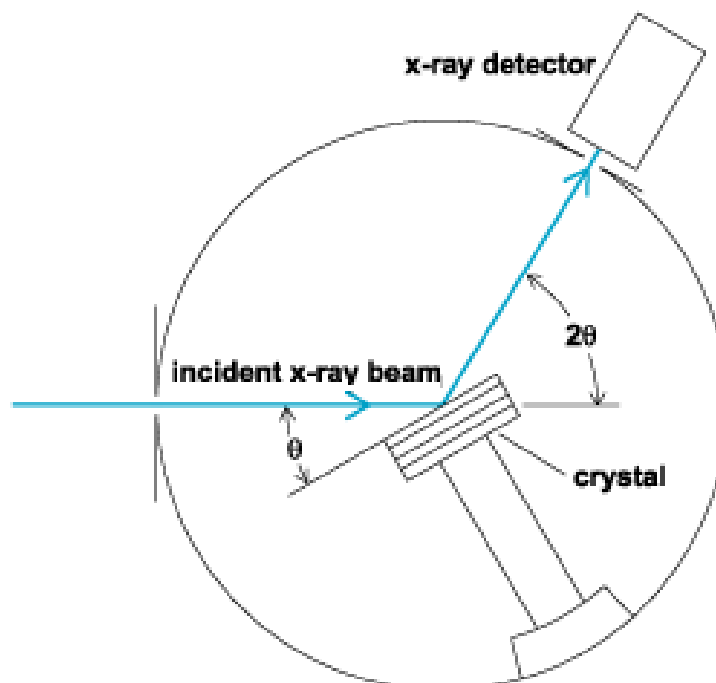


**Figure 2.9:** A simple representation of X-ray diffraction [19]

The linear absorption coefficient of the material for radiation determines the depth of penetration. For instance, in iron, nickel, and aluminum-base alloys, 50% of the radiation is diffracted from a layer approximately 0.005 mm (0.0002 in.) deep. This shallow depth of penetration allows determination of type I, type II and type III residual stresses as functions of depth, with depth resolution approximately 10 -100 times that possible using other methods. One should be careful about choosing the diffraction angle; because material has more than one diffraction peak and the higher the diffraction angle gives the greater the precision. To have meaningful results diffraction angles,  $2\theta$ , greater than  $120^\circ$  is used [18].

There are different techniques of measuring residual stresses states with X-ray diffraction method. These are; the double exposure or two- angle technique (DET), the single exposure or one- angle technique (SET),; and the sin-square-psi or multi-angle technique ( $\sin^2\psi$ ). For this study the last technique was used [17]. The main advantage of the  $\sin^2\psi$  technique, considering the additional time required for data collection, is in establishing the linearity of  $d$  (*lattice spacing*) as a function of  $\sin^2\psi$  to demonstrate that XRD residual stress measurement is possible on the sample of interest [18].

The most common errors for X-ray diffraction measurements are [20]:

- Stress constant selection;
- Instrumental and positioning;
- Process geometry;
- Diffracted peak location;
- Cold-working and microstresses;
- Having texture;
- Large grain sizes;
- X-ray elastic constants;
- Microstructure.

Detailed explanation about XRD and instrumentation will be found in Reference [21].

### 2.2.3 Magnetic Barkhausen Noise

Magnetic Barkhausen Noise was discovered in 1919 by H. Barkhausen when he drilled a ferromagnetic specimen with a wire and hooked it to an external speaker. Residual stress state or the carburization level of the component can be determined non-destructively by MBN. This technique may improve the accuracy of remaining-life.

Barkhausen effect originates from changing magnetic domains of a ferromagnetic material during the magnetization process. Barkhausen found out that the hysteresis curve was not a really linear curve but composed of small jumps as the domain walls break away from pinning sites such as dislocations, precipitates and grain boundaries. This phenomenon is illustrated in the figure below [22] [23].

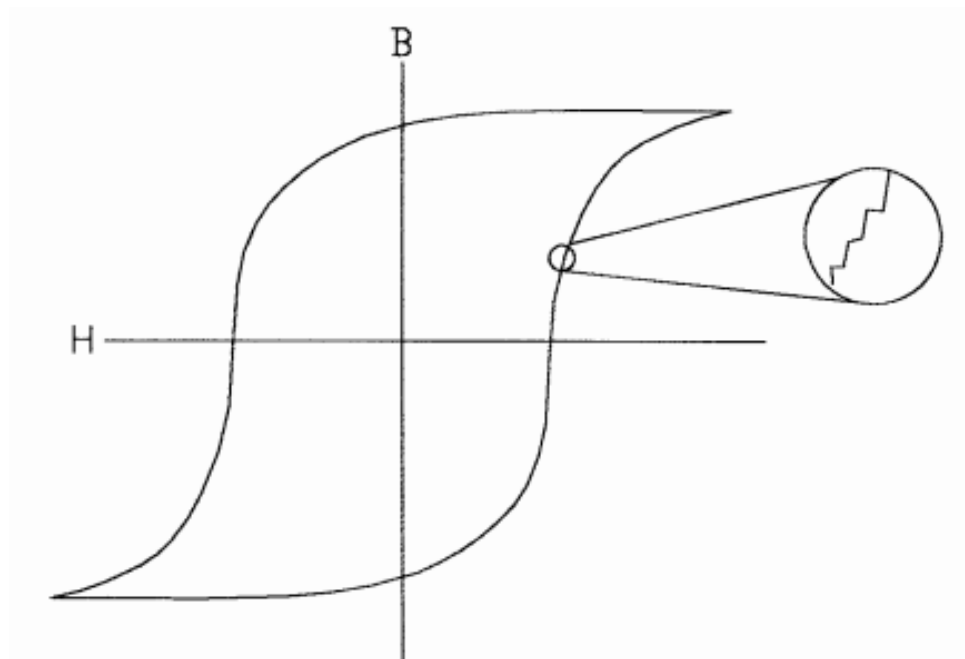


**Figure 2.10:** Flux density (B) curve as a function of magnetic field intensity (H) in ferromagnetic material. The inset shows Barkhausen jumps [24]

MBN measurements need ferromagnetic material, magnetic field and magnetization strength. Examples of ferromagnetic materials are iron (as BCC  $\alpha$ -ferrite), cobalt and nickel. The term magnetic field refers to a field of magnetism that exists between two

magnetic poles and has the ability to exert a force on a ferromagnetic particle that is within the volume of the field. If the field winding current of the system is high, the strength of the magnetic field will be high. Magnetization means to excite the field for obtaining Barkhausen Noise signature [22].

Residual stresses influence the magnetic domain structure of ferromagnetic materials and also the Barkhausen noise. Compressive residual stress reduces the intensity of the Barkhausen noise whereas tensile stress increases the maximum Barkhausen noise level (Fig. 2.11).

Magnetic Barkhausen Noise has two measurement techniques; surface Barkhausen noise and encircling Barkhausen Noise. In this study, the first technique is used which is done by placing the detection coil on the surface of the specimen [23].

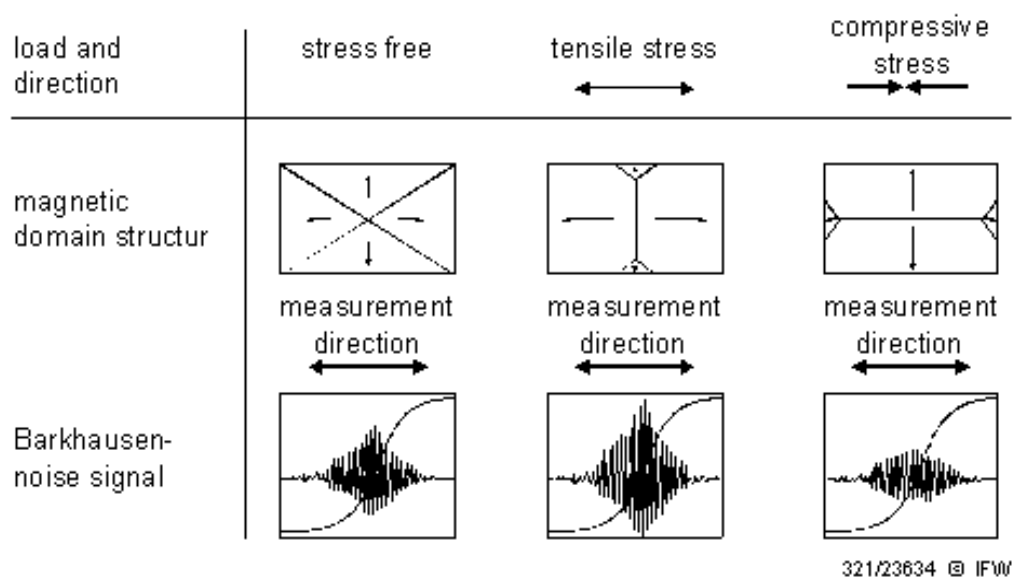


**Figure 2.11:** Barkhausen Noise Levels [24]

The apparatus for the applied stress measurements consists of a magnet, a power supply, a sample, a search coil, a filter/amplifier, a PC and a testing machine.

Changes in microstructure (grain size, texture, phase, etc.) affect MBN behaviour of the sample. Therefore, residual stress distribution measurements are also affected in modified microstructure. In this thesis, it was assumed that the microstructure did not change during forming operations and the MBN results were confidential. Figure 2.13 shows the effect of microstructure on Barkhausen noise.

The effect of microstructural changes on the MBN signals was investigated with various different microstructures. Microscopic observations showed that Barkhausen noise signals were strongly affected by the microstructural changes. It varied inversely with hardness, which indicated that a high hardness value was closely related with increased dislocation density and residual stress which act as a barrier to irreversible domain-wall motion. Moreover, morphological changes in the sample affected the noise level. [28]

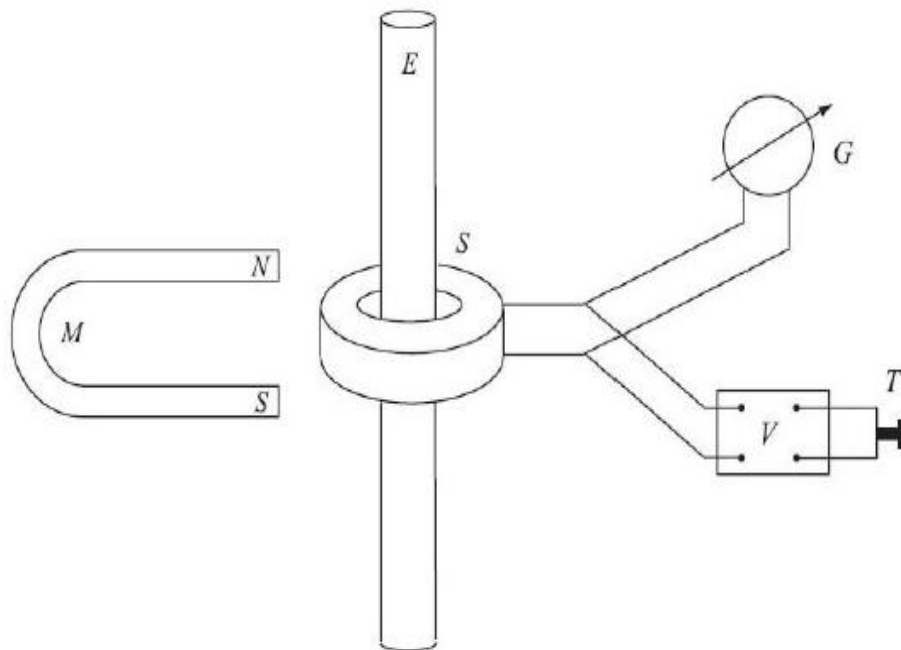


**Figure 2.12:** Experimental set-up of Barkhausen [26]

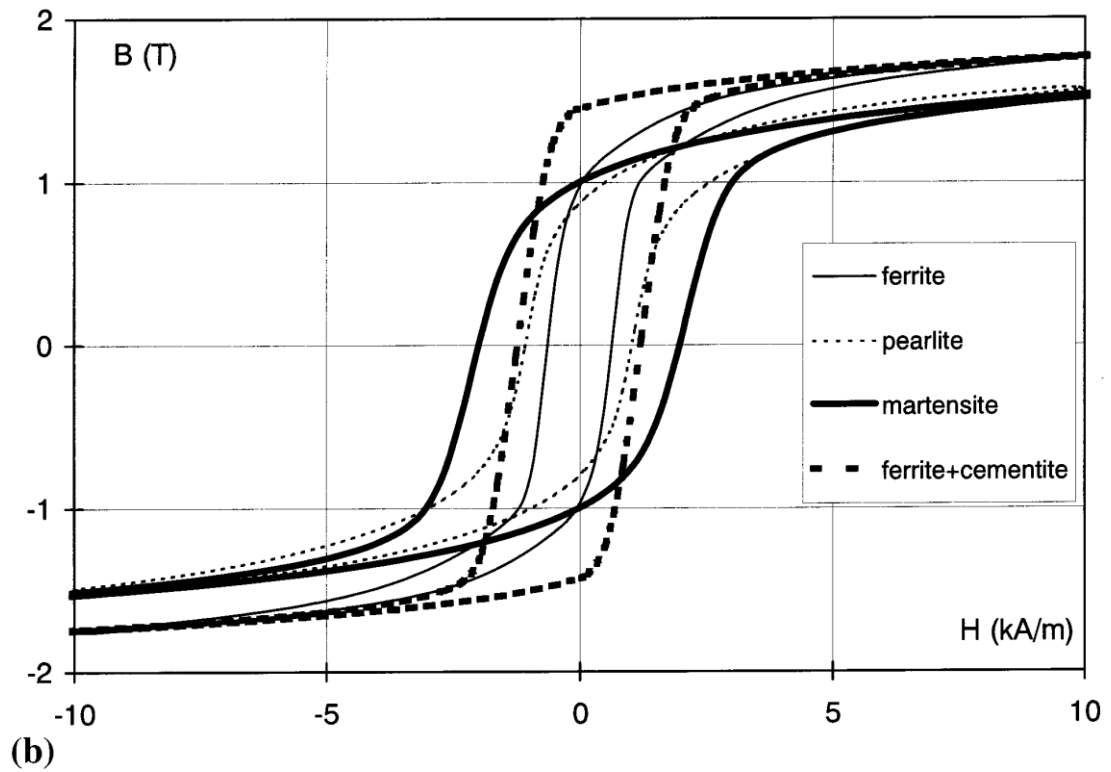


**Figure 2.13:** Effect of microstructure on Barkhausen noise [27]

Some applications of the MBN method are summarized below:

- Residual stresses measurements. Example applications are bearing components, fatigue failure degradable products, aerospace engine components and automotive industry components. [29];
- Hardness and structure state measurement [24];
- Microstructural measurements, including evaluation of grain size measurement;
- Evaluation of anisotropy;
- Measurement of the degree of aging and morphology;
- Measurement of iron loss in magnetic materials [30].

Stress conditions for magnetic inspection can be done by MBN if and only if calibration is made with a nearly identical specimen [31].

## CHAPTER 3

### LITERATURE SURVEY

There are many studies about FEM simulation, deep drawing, magnetic Barkhausen noise measurements and X-ray analysis. However, for the sake of simplicity, some selected studies were included in this chapter by focusing on the frame of this thesis study.

Simulation programs observe simultaneous change in many different parameters was claimed by Miklós Tisza. The emerging role of modelling and simulation is providing shorter lead times, better quality and more cost effective production. In order to do this finite element method (FEM) environment will submit rapid engineering solutions and theoretically more reliable results [32].

A.E. Tekkaya has worked on the same issue. He claimed that the simulation of sheet metal forming processes is both academic and industrial exercise Academic work was the first step and industrial applications are the next [33]. Academic and industrial studies were combined in this thesis.

Determining the finest finite element simulations of deep-drawing operations, including spring-back effect, until the occurrence of strain localisation was performed by O. Incandela. They gave clear information about equivalent stress–equivalent strain relationship and description of boundary conditions. The study devoted to the description of the procedure adopted to evaluate the residual stress and strain by the finite element technique with explicit algorithm. The experimental and the numerical results were correlated with each other [34].

Numerical (FEM) and experimental investigations on the residual stresses were performed by M. Kleiner et al. Combined FEM and experimental investigations have been carried out. A comparison showed a meaningful agreement between the theoretical and experimental results which allow determining the qualitative distribution of the residual stresses [35].

The residual stresses distribution through the sheet thickness in the case of cylindrical deep-drawn part was investigated by C.Axinte and M.Iordache. The experimental and simulation analysis were performed simultaneously. Parallel results of stresses profiles were obtained from the two analysis techniques. Results showed that usually the residual stresses distribution is same for the two cases, but in the centre of the part bottom, stresses determined by simulation are higher compared to those experimentally determined. The error should be caused from using different number of calculation steps through the sheet thickness or the way in which the material parameters were implemented into the analysis programme [36].

Determining residual stress state generated by cold-drawing in a ferritic steel rod was performed by J.M.Atienza et al. Stress profiles were measured by XRD and calculated by 3D finite element simulation. Surface stresses were measured by XRD in many points to confirm the hypothesis of a uniform tensile stress state at the rod surface. A commercial 3D finite element programme was used in order to understand the effects of the drawing process. Experimental and simulation results were in the same manner. In this way, the finite element simulation is a successful tool for anticipating macro residual stress states of the products.

There was significant residual stress state at the surface of the rod. This may affect the mechanical properties by minimizing the elastic limit in the tensile test, increasing the losses in stress relaxation test and reducing service life in case of having stress corrosion cracking and fatigue [37].

FEM simulations in cylindrical deep drawing operation to modify the draw die profile were used in J. Danckert's study. He concluded that the experimental findings of residual stress state are in close agreement with the results obtained using FEM [38].

Finite element simulations in order to study the influence of bearing geometry on the residual stress-state in cold drawn wires were performed by Henrik Överstam. XRD experiments have been performed in order to verify the FEM results. The residual stresses were measured in both the axial and tangential direction. It was found that geometry of the bearing has a large influence of the residual stress-state. In the tapered bearings the stress state measurements were low or compressive. Simulation results showed that a small taper in the bearing also gave low or compressive stresses [39].

XRD residual stress measurements of deep drawn 301 LN unstable austenitic stainless steel were done by M.R. Berrahmoune et al. Macroscopic tangential residual stresses were determined after deep drawing at different drawing ratios. Mentioned parameters increase with increasing drawing ratio and the maximum is located in the middle of the cup height. These stresses will be correlated with local measurements to understand how the stress is distributed in deep drawing cup [40].

Residual stress measurements with magnetic Barkhausen noise (MBN) were performed by D.M. Stewart et al. MBN is a triumphant example of non-destructive testing technique for determining residual stress in steel. In this study AS1548-7-460R steel was used. The sample under applied stress showed a clear asymmetry between compression and tension [23].

Barkhausen noise analyses (BNA) were studied by J. Thomas et al. They concluded that Barkhausen noise was an effective tool for evaluating changes in microstructure of ferromagnetic materials. Using advanced techniques BNA can also effectively locate and estimate the magnitude of subsurface stress features. They also performed series of experiments on XRD and MBN correlations. [41].

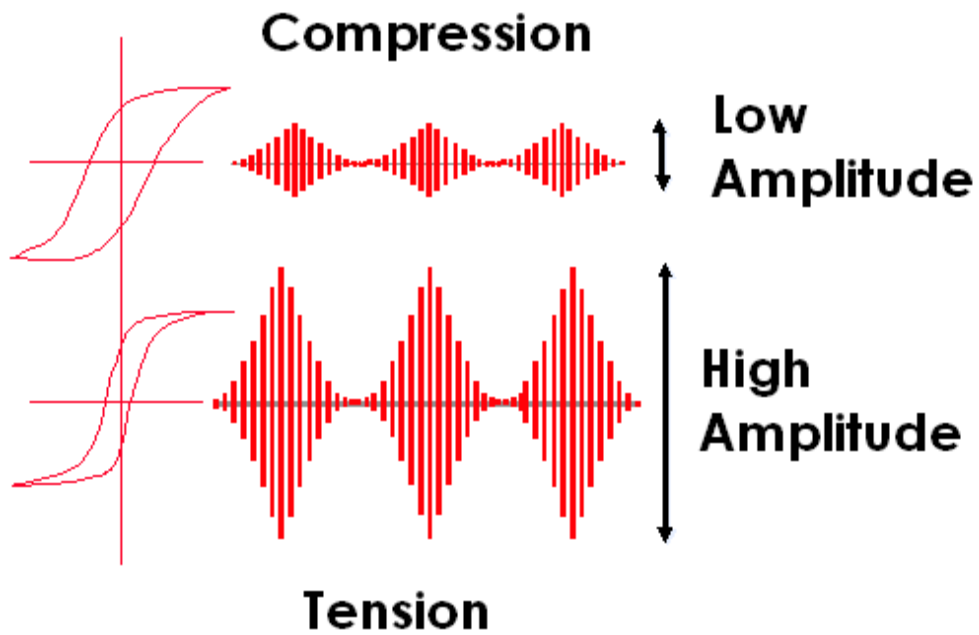


**Figure 3.1:** As tensile residual stresses increase the amplitude of the Barkhausen noise bursts also increase [41]

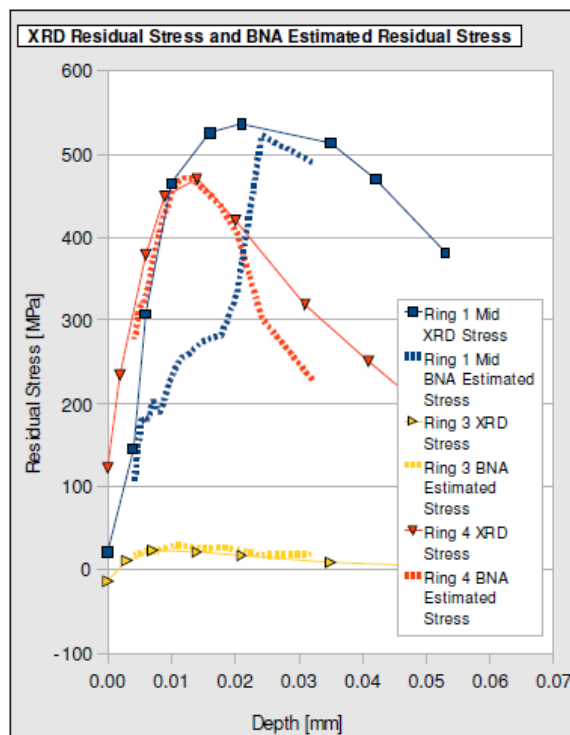


**Figure 3.2:** Residual stress depth profiles measured with X-ray diffraction and estimated with Barkhausen noise analysis [43]

The magnetic Barkhausen noise (MBN) in deformed low alloy steel was studied by M. Blaow et al. As confirmed by X-ray diffraction measurements, one effect of plastic deformation is to leave a residual compressive stress on the tension side of the specimen and a residual tensile stress on the compression side. Measurements of residual stress were correlated with MBN peak height, to the extent that both quantities show functional forms similar to the theoretical relationship between residual stress and deformation process [42].

An experimental study about comparing magnetic residual stress measurements with X-ray diffraction analysis were performed by J. Epp et al. AISI 52100 steel ball bearing rings with various and inhomogeneous residual stress states have been investigated. Reliable results and good agreement between X-Ray diffraction data and residual stresses calculated from the magnetic analysis was obtained with the use of a calibration for each single component. A single-part-calibration gives satisfying results with a gain of time from 50% to 90%, compared to X-ray diffraction. Although, there exist disagreements on magnetic residual stress measurement technique the errors are in the range of the standard error given by X-ray diffraction. The magnetic measurement technique represents an important gain of time compared to standard X-ray diffraction measurement. [43]

## CHAPTER 4

### EXPERIMENTAL PROCEDURE

#### 4.1 Material

In this thesis cold rolled St4 steel was used. It corresponds to EN10130-DC04 in Euronorm, NFA 37-501- F14 in France, DIN 1624-St4 in Germany, BS 1449-CS1/CR1 in UK, ASTM- SAE 1006 in USA. Chemical composition of St4 is given in table 4.1 [44].

**Table 4.1** Chemical Composition

Element	C	Si	Mn	P	S	Cr	Mo	Ni	Cu	Al	N
Weight%	0.037	0.001	0.124	0.007	0.012	0.009	0.002	0.010	0.013	0.041	0.006

Forming cycle of the St4 steel was started with cold-rolling then continues with annealing and the final stage was temper rolling (skin rolling). The initial mechanical properties of the material are showed below by two set-tensile test data (Figure 4.1 & Table 4.2)

**Table 4.2** Anisotropy Coefficient of St4

	<b>R</b>	<b><math>\Delta R</math></b>
1-0° wrt rolling direction	1.24	1.11
1-45° wrt rolling direction	0.8	
1-90° wrt rolling direction	1.59	
2-0° wrt rolling direction	1.28	1.20
2-45° wrt rolling direction	0.79	
2-90° wrt rolling direction	1.44	

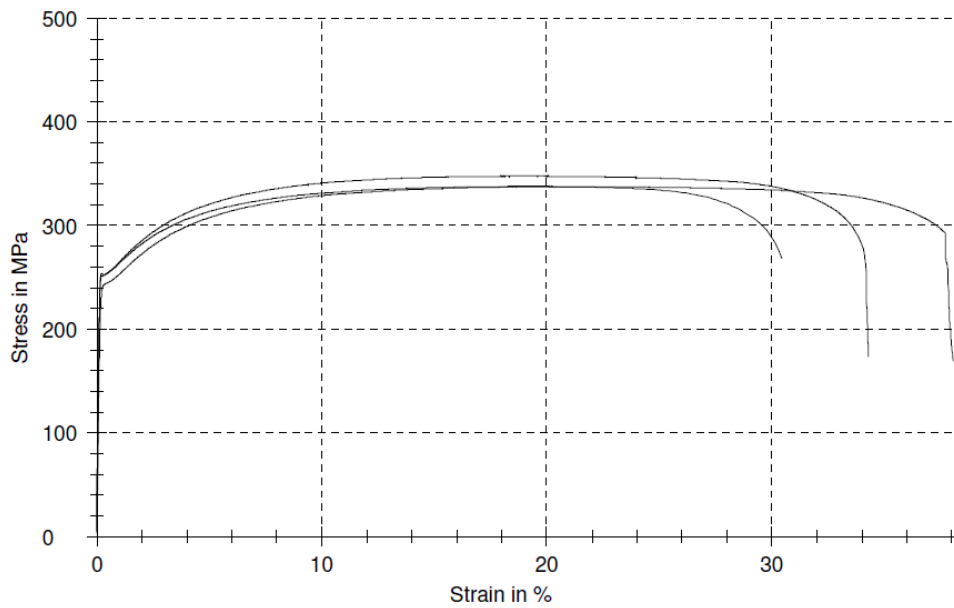


**Figure 4.1:** Tensile test data of St4 cold rolled steel sheet

The different material characterization methods were used for this study. Tensile Test, Compression Test, Hydraulic Bulge Test and Nakazima Test were done for obtaining data for Finite Element Program, because its library does not possess all the materials' flow curves or other specific properties.

Hardness investigation and microstructural examinations were made on samples before and after deep drawing and bulging operations. Results of these experiments showed the history of the samples and helped us making comments on variation residual stress state. These methods are briefly explained in this section. Test equipments and some detailed information about the aim of the method are discussed at the same time.

## 4.2 Tensile Test

Tensile test is one of the keys of material characterization methods. Due its simplicity and ease of application, it is the most common technique. Although it is common and useful, some other methods have been developed because of some limitations of simple tension test.



**Figure 4.2:** Zwick/ Roell Z300E All-round Universal Testing Machine  
Below some properties of test machine can be seen in Table 4.3 [45]

**Table 4.3** Properties of Zwick/ Roell Z300E

Fmax [kN]	300
Number of lead columns	4
Number of drive columns (ball lead screws)	2
Stiffness of load frame crosshead deflection and elongation of lead screw drive approx. [kN/mm]	450
including load cell, hydraulic grips and drive approx. [kN/mm]	200
Dimensions of load frame H1 – Height [mm]	2600
B1 – Width [mm]	1145
T1 – Depth [mm]	845
Dimensions of test area H2 – Height [mm]	1800
B2 – Width [mm]	630
Test stroke max. without tools / specimen grips [mm]	1630
H3 – with hydraulic grips 8595 (including load cell) [mm]	1115
H4 – with wedge grips 8520 (including load cell) [mm]	830
Test speed [mm/min]	0.001-250
Weight without tools / specimen grips (with electronics) [kg]	2000
with specimen grips [kg]	2600
Specific floor loading [kg/cm <sup>2</sup> ]	4
Position accuracy [ $\mu$ m]	0.5
<b>Environmental conditions</b>	
Operating temperature [°C]	+10 ... +35
Storage temperature [°C]	-25 ... +55
Humidity range (not condensing) [%]	< 90
Electrical connection Mains voltage 3 Ph/N/PE 2 3 [V]	400
Mains frequency [Hz]	50/60
Drive power without specimen grips [kVA]	6
with hydraulic grips [kVA]	1
Fuse [kW]	9
	16

In this study, the tensile tests for St4 cold rolled steel were performed to obtain stress-strain curve. Moreover, anisotropic behavior of the sheet metal was obtained by testing with samples prepared in 0°, 45° and 90° with respect to rolling direction

Zwick/ Roell Z300E All-round Universal Testing Machine was used during tensile tests in Atılım University Metal Forming Center of Excellence (MFCE). The machine is shown in Figure 4.2.

Specimens of the St4 cold rolled steel were prepared by wire erosion device. Totally 2 sets of specimens used, which are from 3 different directions.

Tensile tests were performed with a tool speed of 250 mm/min at room temperature. Each test is repeated for three times for three directions with respect to rolling direction to obtain anisotropy properties of the material.

Test data is analyzed by Zwick *testXpert*® software. Some assumptions were used for obtaining best flow curve. These assumptions and results are given in Chapter IV.

### **4.3 Compression Test**

Compression tests were done with Zwick/Roell Z300E All- round Universal Testing Machine. Test sample diameter was 15mm. The thickness of the sheet was 1.8 mm and 4 sets of test were performed. In these tests 5 sheets were stowed and the final shape assumed as bulk material with 9 mm height. The same software program was used for analyzing.

### **4.4 Hydraulic Bulge Test**

Tensile and compression tests' results are limited, because of giving low strain values. One should interpolate these, and the results of interpolation may not be parallel if we compare to a real case. These tests are done in one dimension, but

hydraulic bulge test is a two- dimensional. In sheet forming operation biaxial as well as uniaxial stress state exists [46].Therefore, one can obtain plastic behavior of the sheet metal for high strain values. Flow curve from the hydraulic bulge test is preferential than the others in Finite Element programs.

The strain hardening properties of the sheet materials in biaxial tension are generally determined by the hydraulic bulge. In the bulge test, flow curve of the sample can be derived up to failure of the sample, however in the conventional uniaxial test only the uniform strain range can be utilized. The bulge test can better characterize the plastic properties of sheet metal at large strains, because the strains in press forming are normally larger than the uniform strain. This is very important in determining the stress-strain behavior of sheet metals, which are produced by cold-rolling like St4 steel.

During the hydraulic bulge test first step is expanding the sheet metal with internal pressure while the edge of the sheet is held firmly to prevent axial movement. The next step is measuring the internal pressure and bulge height continually during expansion. Converting the data into the true stress-strain data using analytical equations is the third step. The last but the not the least important step is using the least-squares method to fit the data into known and widely used equation forms to obtain a flow stress curve that is easy to use [47].

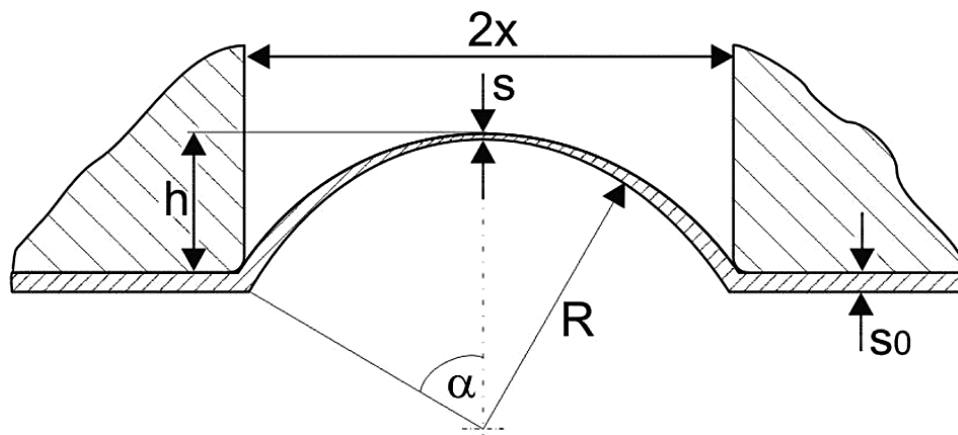


**Figure 4.3:** Geometric parameters of hydraulic bulge test study [46]

The bulging pressure (P) and the dome height (h) values and Von Misses's theory of plasticity were used for calculating the flow stress/curve. This theory based on some assumptions:

- The bulge shape is spherical;
- No material is drawn into the die cavity;
- The sheet is thin and the bending stress could be ignored;
- The effect of the die corner radius (Rc) is negligible when  $R_c < D_c/20$  ( $D_c$ ; bulge diameter);
- The material property is isotropic and follows the Von Misses yield criterion.

With these assumptions, the equivalent stress ( $\bar{\sigma}$ ) and strain ( $\bar{\epsilon}$ ), the curvature of the bulge radius (R), density ( $\rho$ ) and the thickness (t) could be calculated using the following equations [48].

$$R = \frac{D_c}{2} \quad (4.1)$$

$$\bar{\sigma} = \frac{P\rho}{2t} \quad (4.2)$$

$$\bar{\epsilon} = \ln \left( 1 + \frac{h^2}{R^2} \right) \quad (4.3)$$

$$t = t_0 \frac{R^2}{2\rho h} \quad (4.4)$$

Experimental works were performed for 1.8 mm St4 cold rolled steel. Zwick/Roell BUP600 Erichsen Testing Machine was used. This fully PC-controlled multi-purpose hydraulic sheet metal forming machine, is designed for formability testing of sheet metals in accordance with the most common standards and procedures.

The Zwick/Roell BUP600 Erichsen Testing Machine has a 600 kN load capacity, a maximum clamping force of 50 kN, a maximum test stroke of 120 mm, and a maximum test speed of 750 mm/min. One can perform earing tests, Nakajima and

Marciniak-Kuczynski formability tests, square cup drawing tests, and bulge tests [49].

The system consists of an upper and a lower dies, pressure transducer and cover mica to prevent oil leakage. Upper and lower dies have approximately 150mm diameter drawbead. These dies prevent material flow in clamping region.

The sample was prepared by applying coating on it. The coating markers were used as reference points. According the movements of these during hydraulic bulge test, the flow curve was obtained by GOM-ARAMIS, which is Digital Image Correlation system. This system provides better understanding in material and component behavior and is ideally suited to monitor experiments with high temporal and local resolution.

Statically or dynamically loaded test objects can be measured by ARAMIS which is a non-contact and material independent measuring system. It is the ideal solution for, determination of material properties (R- and N-values, FLC, Young's Modulus, etc...), component analysis (crash tests, vibration analysis, durability studies, etc...) and verification of Finite Element Analysis. Furthermore, the system is the unique solution delivering complete 3D surface, displacement and strain results where a large number of traditional measuring devices are required.

According to these technical data, one can see that ARAMIS system has very special cameras so that accurate deformation stage measurements were obtained. During this study 2 cameras were used to determine the data [50].

Hydraulic Bulge Testing Steps:

- High viscosity fluid fills the lower die.
- Transparent mica is placed between upper die and high resolution CCD cameras (ARAMIS) in order to viscous fluid splashed during fracture of the sample.



**Figure 4.4:** BUP 600 hydraulic press with GOM ARAMIS

- Led lamps are set to eliminate reflection of the viscous oil and provide necessary media for CCD cameras.
- The deformation procedure is recorded up to fracture stage. Generally at least 400 photos are recorded. At the same time, computer controlled hydraulic press results are recorded with 0.01 second time interval.
- Different nodes over the crack region are selected to collect data.
- Displacements along x, y and z-directions are obtained. These results are recorded and the software program calculates stress and strain values according the analytical and numerical formulations.

Stress- strain behavior of the St4 cold rolled steel due to this test is given in next chapter.

#### **4.5 Nakajima Test**

The Forming Limit Diagram (FLD) gives process limitations in sheet metal forming and is used to investigate the stamping characteristics of sheet metal materials. For planning safe and secure deep drawing process, forming limit diagram is a necessary guide. It gives the failure map of the material in terms of major and minor principle strains.

The FLD indicates the relationship between these principal strains under diffuse or localized necking in a plane-stress condition for different strain paths. FLD of sheet metal is usually obtained based on localized necking. For a sheet metal under stretching load, diffuse necking can be observed at first, and then localized necking appears. Within the localized necking process, the sheet thickness decreases sharply, then the sheet failure occurs. Hence, the major and minor strains when localized necking initiates are described as forming limit strains of the sheet [51].

The Nakajima test is a known method to determine the Forming Limit behavior of sheet metal materials. The method is based on the principle of deforming sheet metal blanks of different geometries using a hemispherical punch until fracture occurs (Fig. 4.6).

In this study, 6 different geometries were used. Each specimen has 6 different radius values, between 40 to 100 mm. Specimen shape is shown in Figure 4.7, it changes according to different deep draw and stretch forming conditions occur on the sheet metal surface (from a regular biaxial deformation to a simple tensile load) so different strain ratios were obtained. Specimen with 40 mm radius is the smallest specimen and characterize simple tension load. Specimen with 100 mm radius is the biggest specimen and biaxial strain condition is obtained with the full geometry specimen. The other specimens gave intermediate strain ratios. Results are given in Chapter V [48].

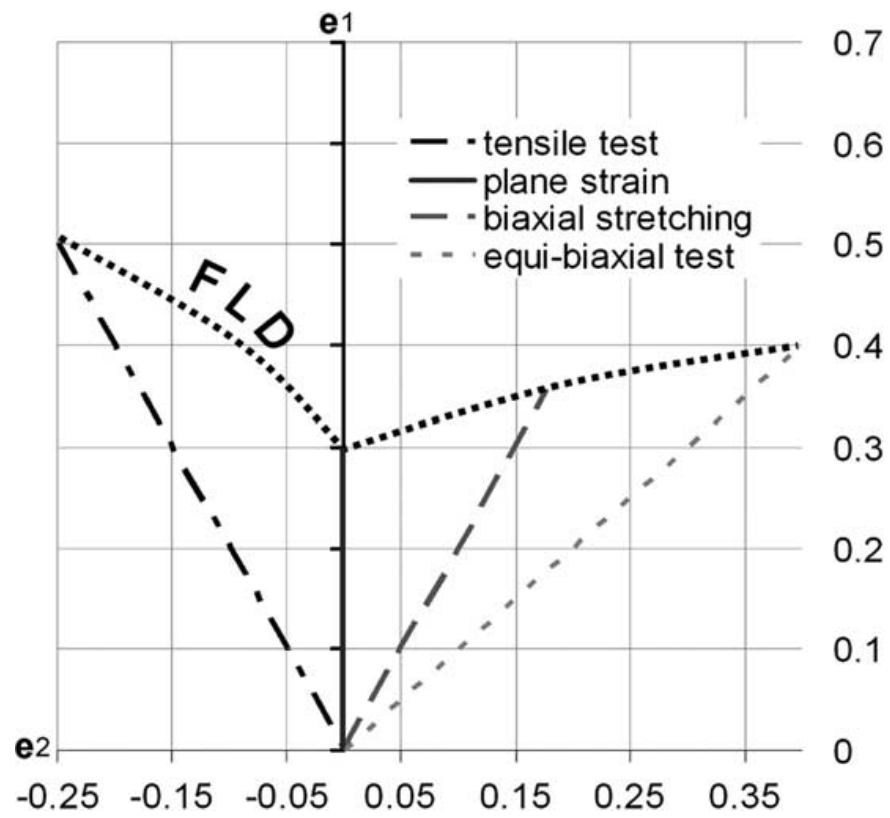


**Figure 4.5:** Typical forming limit diagram [51]

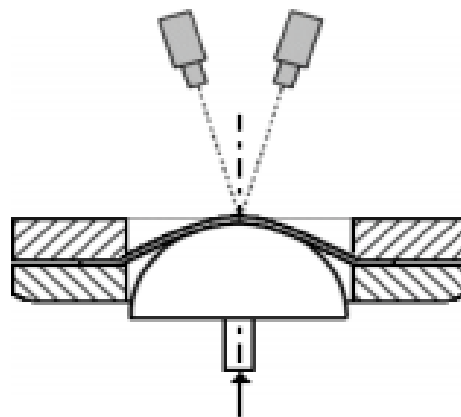


**Figure 4.6:** Nakazima test arrangement [52]

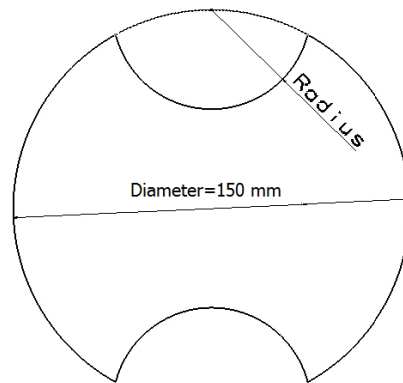


**Figure 4.7:** Nakazima test specimen

Specimens for the tests are prepared by wire erosion so any kind of microcracks, geometrical and dimensional defects are eliminated. The sample should be etched before the test. These etched points give the displacement data for FLD. Figure 4.8 shows an example of the etched sample



**Figure 4.8:** Etched sample

Nakazima test was done by GOM-ARAMIS system. As mentioned before it is used for fast and accurate measurements. ARAMIS compares the instantaneous images with the initial digital image and calculates the displacement and the deformation of the object characteristics. ARAMIS automatically divides the etched sample's image into small overlapping areas (squares or rectangles) and defines the corresponding area in the stereo image. Sophisticated calculation methods provide for assigning the corresponding area ultra-precisely (sub pixel range). By assigning all image details to the stereo image, the shape of the sheet metal in its reference state is measured based

on the calibration data of the system. Nonetheless, the image details of the reference image can be allocated to the images of the recorded subsequent stereo image pairs. Thus, the shape and the deformation of the sheet metal was precisely recorded and measured for each recording moment after the automatic evaluation.

The whole deformation behavior of the sample material during forming and fracture processes are obtained and reported as final data by recording and evaluating numerous images with the corresponding load parameters (force and deviation) during the forming process.

ARAMIS calculates the characteristic values (theoretical maximum of major and minor principal strain) by the computation of an ideal shape of the curve from the captured measuring values. Each different sample's (different radius) forming behaviors at material failure were performed for 3 times.

The measuring points (major and minor strain) averaged from the different specimen geometries are now connected and thus allow for designing the Forming Limit Diagram of the currently tested material. Using ARAMIS, deformations and strain can easily and precisely be measured. Installing the system above BUP 600 provides for efficiently and reproducibly captures Forming Limit Diagrams.

For obtaining FLD diagram of the St4 cold rolled steel, BUP600 and GOM-ARAMIS were used together. Applications of Zwick/Roell BUP 600 were described above. During the test a rigid punch was used instead of oil that is used in bulge test.

#### **4.6 Residual Stress Measurements by X-Ray Diffraction Method**

Seifert XRD 3003 PTS is the X-ray diffraction (XRD) system was used to measure the residual stress state of cold rolled St4 steel. Measurements were done in Atilim University, Metal Forming Center of Excellence.

The system consists of X-ray tube, goniometer, texture-stress attachment, x-y stage and detector. The tube is the X-ray source, for this study Cr tube was used. Cr radiation has a wavelength of  $2.28970 \text{ \AA}$  and the maximum power rating of the tube can handle is 1.9 kW.

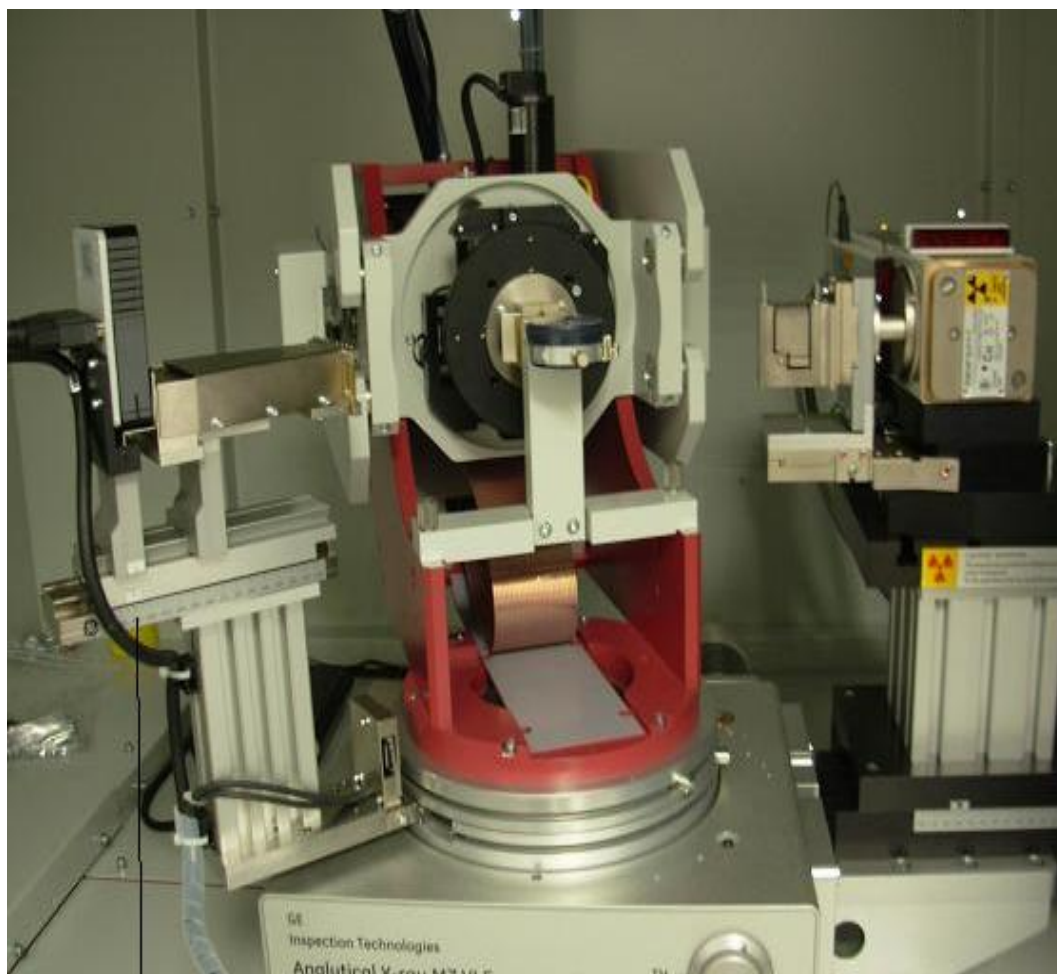


**Figure 4.9:** Seifert XRD 3003 PTS

The X-ray is sent to a specified point by point collimator. To have more accurate results, little diameter collimators should be used. 2mm, 1mm and 0.5 mm diameters collimators were used and optimum results were obtained with collimator with 0.5 mm.

Goniometer, texture- stress attachment (TSA) and x-y stage provides 7 different movement axes. Therefore, one can easily measure the residual stress state of any point. During measurement 40 kV voltage and 40mA current is applied. The detector is a Pulse Sensitive Detector (PSD) and capable of counting 50000 pulses per second.

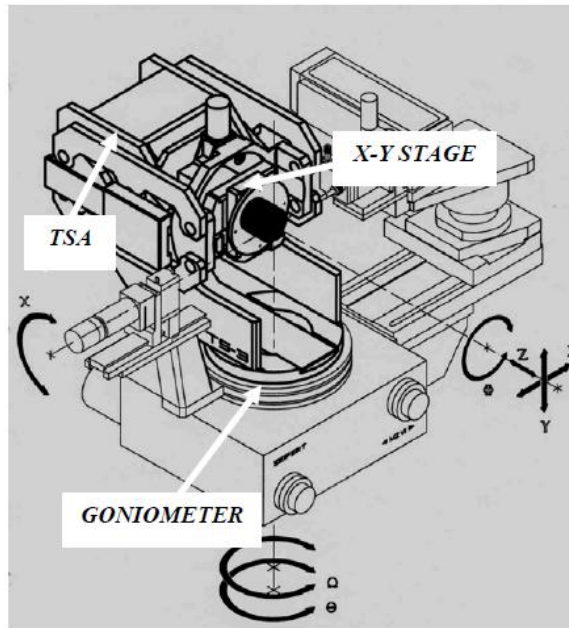


**Figure 4.10:** Goniometry, TSA and X-Y Stage [53]

$\theta$  axis budges the detector and  $\Omega$  axis budges the goniometer. Measurements were done in  $\theta$ -2 $\theta$  interval. X, Y and Z axes were used for centering the point which wanted to be measured. The other axes were responsible for measurements at different directions.

Measurements were done in these steps:

- Specimen was mounted on the goniometer. For obtaining the X-ray at the specified point, the X, Y and Z axis were used. No sample preparation was need.
- The  $\theta$  axis was stated between  $148^\circ$  and  $164^\circ$ , because the largest peak value is near  $156^\circ$ .

- 2 different angles were stated for  $\phi$  axis to determine stress tensor.  $0^\circ$  and  $90^\circ$  were given angles.
- There were 26 scans and each of them took up time about an hour.

After measurements were done, analyzing step was started. Diffraction peak positions of 26 scans were used for obtaining residual stress state of the sample. In order to do these derivations special software “SEIFERT, Rayflex Analyze” was used.

During this stage, corrections were made by using some methods which were in the software program. These are Lorentz, Polarization, Background corrections and Smoothing. Details of the methods are in reference [54].

Measurement was finished with determining the peak point and calculating residual stress values. Parabola fit above a threshold value and Center of gravity, mean value methods were used. The results showed that they are parallel. Parabola fit above 50% was used for the first method. In the second one bottom threshold and top threshold values were 30%, 80% respectively. 5% was the step size value.

Residual stress value was determined according to  $\sin^2\psi$  method with linear regression evaluation. After using some assumptions and formulas, the residual stress state was obtained by the below formula. Detailed derivations are in reference [18].

$$\sigma_\phi = \left( \frac{E}{1+\nu} \right)_{(hkl)} \frac{1}{d_0} \left( \frac{\partial d_{\phi\psi}}{\partial \sin^2 \psi} \right) \quad (4.6)$$

Error estimation of this measurement depends on material type, measurement time, axes, collimator diameter, analyzing method etc. Moreover, the system has  $\pm 30$  MPa error by itself.

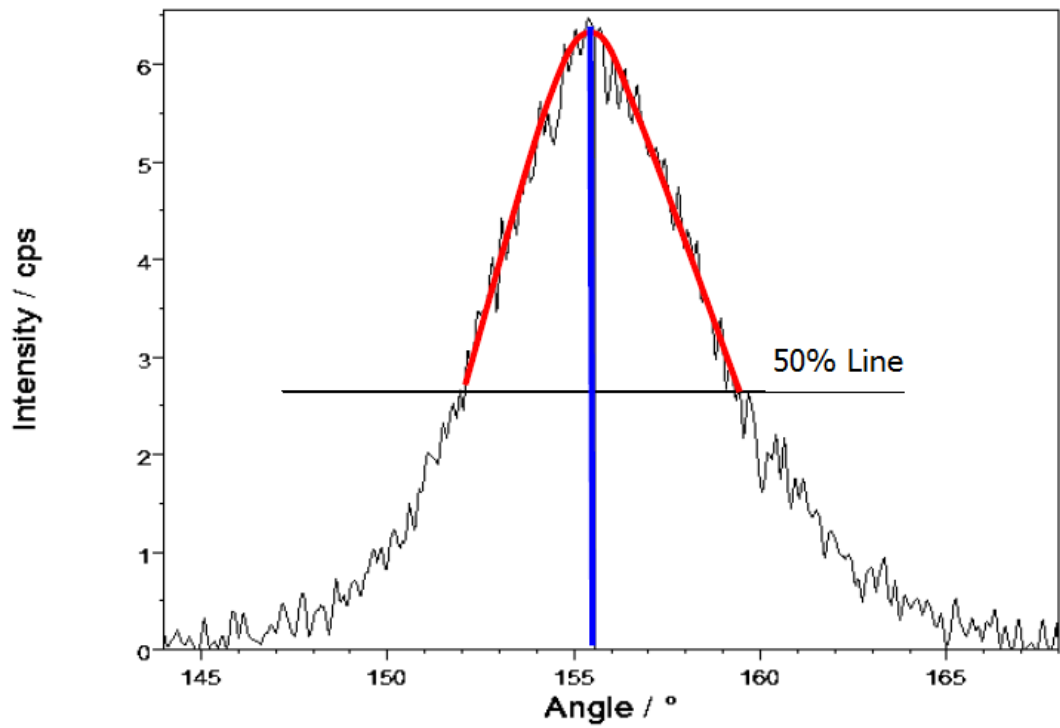


**Figure 4.11:** Parabola Fit method graph

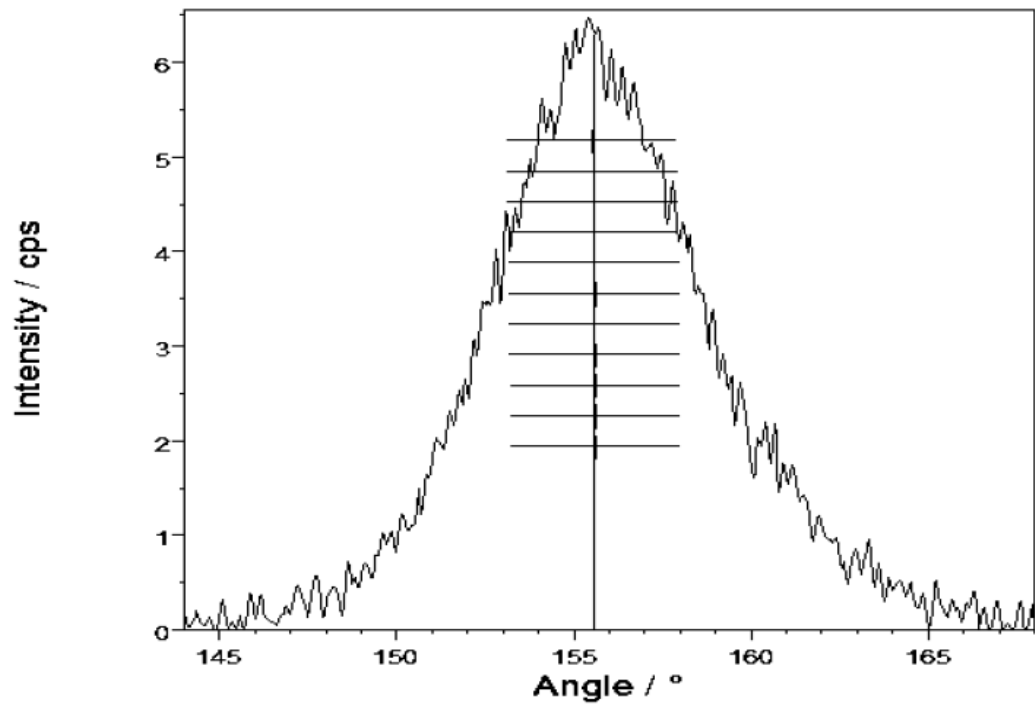


**Figure 4.12:** Center of Gravity method graph

#### 4.7 Residual Stress Measurements by Magnetic Barkhausen Noise Method

Residual stress measurements for bulged sample were carried out by Stresstech Rollscan -  $\mu$ scan 500-2 device (Figure 4.13) and S1-138-13-01 probe (Figure 4.14). The system was connected to computer for obtaining exact values, because the monitor of the device can not show high values above 200 MBN. Measurements were done with 125 Hz magnetic field. Magnetizing voltage was 10 V. Analyze was made by special software program and before analyzing all signals were filtered in the range of 1-400 kHz.



**Figure 4.13:** Stresstech Rollscan- $\mu$ Scan 500-2 device Magnetic Barkhausen Noise Equipment

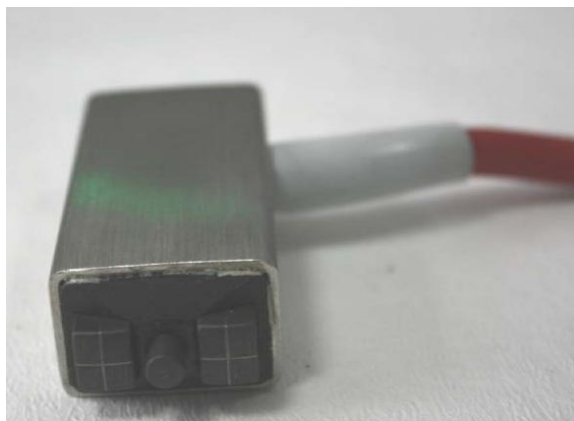


**Figure 4.14:** Magnetic Barkhausen noise probe

First, undeformed sample was measured to optimize the lateral measurements. Undeformed sample was St4 cold rolled sheet metal with 1.8 mm thickness. The surface area of the blank was 190x230 mm<sup>2</sup>. The first measurements showed that, no normalization process was needed for residual stress homogenization. The results are given in the next chapter. Experiments displayed that probe position and contact were very important. Therefore, full contact was obtained and 2 measurements, in rolling direction and normal to the rolling direction, were done for each point.

Calibration tests were performed for two reasons. First one was to find the optimum measurement parameters for experiments. Amplification and magnetization parameters were optimized and during measurements 50 Amplification and 10 Magnetization were used.

Second was to determine relation between MBN and stress. MBN-stress calibration curve was obtained by tensile test machine. Load was applied on a specific sample, during this operation MBN values were recorded by the system. Then, stress values were derived from known load area ratios. These were all done in elastic region. These calibration data is given in next chapter

#### **4.8 Finite Element Simulations**

MSC Marc Mentat and Simufact.forming were used in this study. In this section brief information about the programs is given. Results are shown in the next chapter.

These programs capacitate the metal forming engineer to enable process. The metal forming engineer may use the programs to have important information about material flow, temperature distribution, defects due to improper flow, etc. This can be used to redesign the process in order to obtain the required final geometry and material properties at the desired loading condition.

However, in order to simulate a process on the computer, the problem must be represented on the computer. This action is called modeling. The main steps involved

in this process are choosing analysis type, creating the geometry, defining material properties, initial condition, work piece and dies, choosing remeshing scheme and parameters, defining forming presses and stages using load case, completing the model definition and submitting the job. The numerical simulation cycle is shown in Figure 4.15.

This process can be traversed more than once for a particular design; that is, if the results do not meet the initial estimation, one can return to either the conceptualization or modeling phase to redefine or modify the process [55].

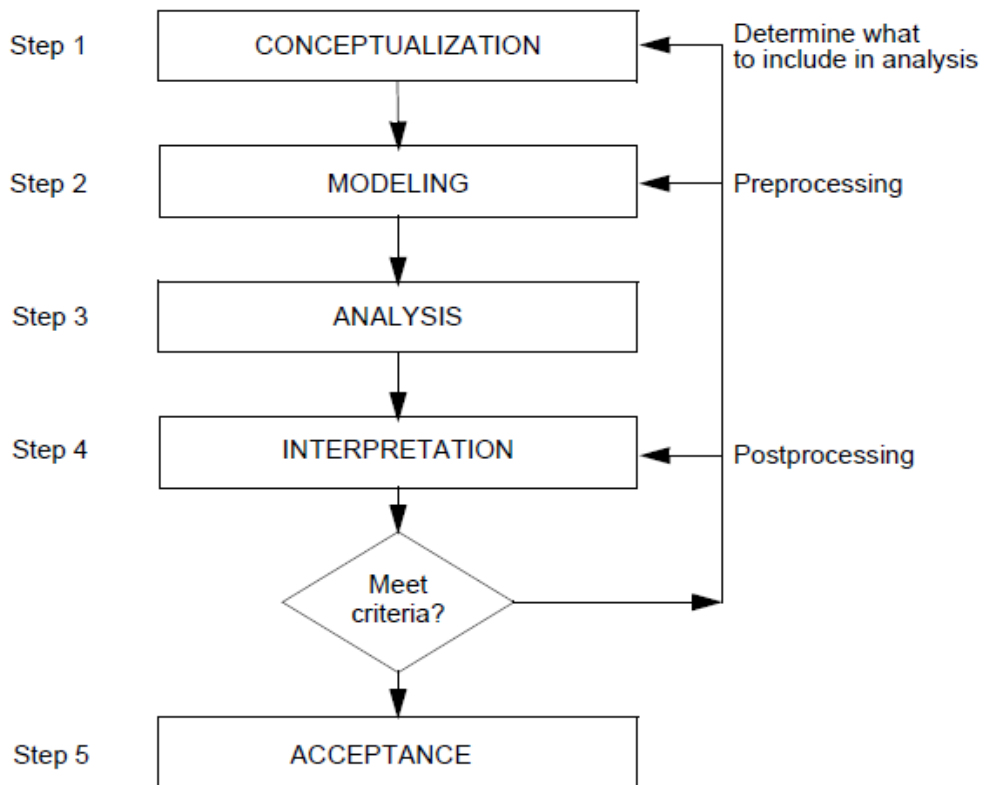


**Figure 4.15:** The Numerical Simulation Cycle [56]

#### **4.8.1 MSC Marc Mentat**

Structural mechanics, heat transfer, and electromagnetic engineering problems can be solved by MSC Marc Mentat program. Marc is used to perform linear or nonlinear stress analysis in both static and dynamic regimes. Physical problems in different dimensions can be modeled by using different types of elements. MSC Marc Mentat has a large variety of mesh generators, graphics, and post processing capabilities, which helps one in the preparation of input and the interpretation of results.

Marc Mentat prepares and processes data for use with the finite element method. It can significantly decrease the time needed for analysis by the numerical method. Graphical presentation of data further reduces this effort by providing an effective way to review the large quantity of data typically associated with finite element analysis [56].

#### **4.8.2 Simufact.forming**

Simufact.forming is a simulation tool, designed especially for the metal forming industry. Therefore, the intention of the program is to provide innovative state-of-the-art simulation technology, which means “optimization of manufacturing processes – adjusted to shop-floor requirements”. Simufact.forming covers a wide scale of challenges in the metal forming industry. From forging to rolling, from metal sheet to massive parts, it offers an integrated simulation environment in each metal forming process, independent from process temperature, the press or the material.

Simufact.forming simulation environment can use the powerful, non-linear solver technologies MSC.Marc and MSC.Dytran. It supports finite elements as well as finite volume analyses. A complete and powerful pre and postprocessor is of course included. Furthermore, all general and the most important native CAD interfaces are supported. [57]

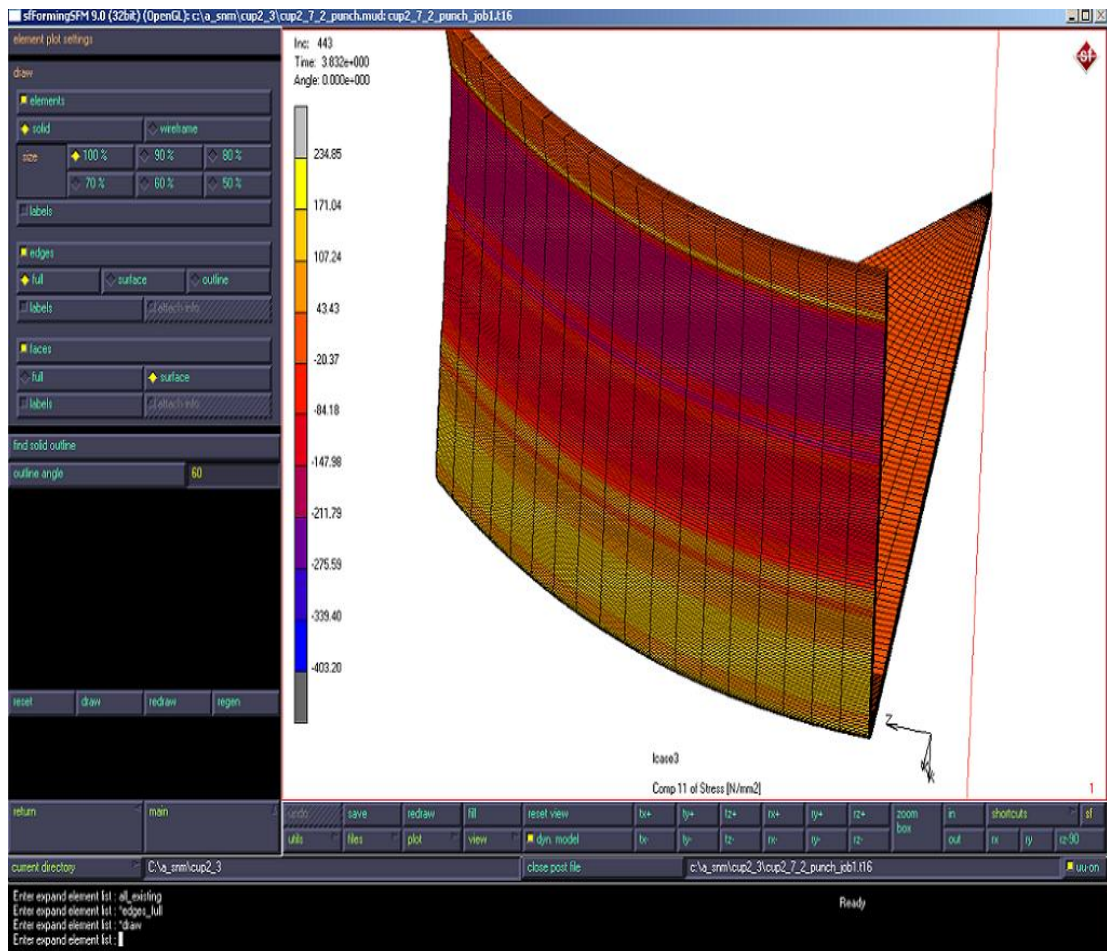


**Figure 4.16:** User interface of Simufact.forming

## 4.9 Experimental Procedure History

Table 4.5 gives the data about the number of experiments and where they performed. Experiments were done in Middle East Technical University (METU) and Atılım University (AU).

**Table 4.4** Experimental Statistics

<b>Experiments</b>	<b>Number of Experiments</b>	<b>METU</b>	<b>AU</b>
Tensile Test	2 sets each has 3 samples (0°,45°,90° rolling direction)		
Compression Test	4 sets each has 5 samples		
Hydraulic Bulge Test	3set		
Nakazima Test	3 set each has 6 samples		
XRD Measurements	70 from 5 different samples in two directions		
MBN Measurements	3 from 2 samples in two directions		
Metallographic Examination	2 from each magnification		
Hardness Test	30 from 2 samples		

## CHAPTER 5

### RESULTS AND DISCUSSION

#### 5.1 Mechanical Tests to Determine Input data for Simulation

Tensile, compression and hydraulic bulge tests were performed to obtain the necessary input data for finite element software. Swift and Voce hardening laws were used in tension and compression test results, and 30-node assumption was used in the results of the hydraulic bulge test (HBT) to establish the flow curves. Stress versus plastic strain data were also obtained from each test.

Moreover, Nakazima test was performed to establish forming limit diagram (FLD) of the cold rolled St4 sheet. Six different geometries were used to obtain this diagram as it is explained in section 4.5.

Figure 5.1 and 5.2 shows the tests results. HBT, tensile and compression tests gave very similar flow curves. According to the flow curve information material constants like elastic modulus, yield strength etc. were obtained for both experiments and numerical measurements. Forming limit diagram provided the failure zone information. Below 0.2 major strain values, safe zone was obtained (Figure 5.2).

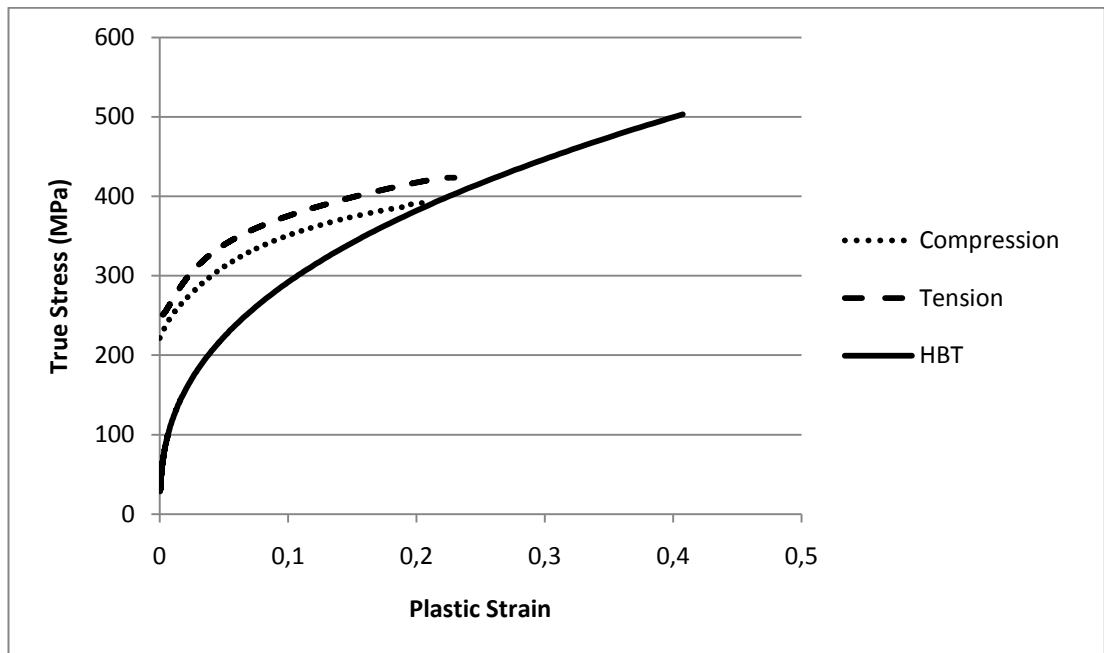


**Figure 5.1:** Comparison of hydraulic bulge, tension and compression test results.

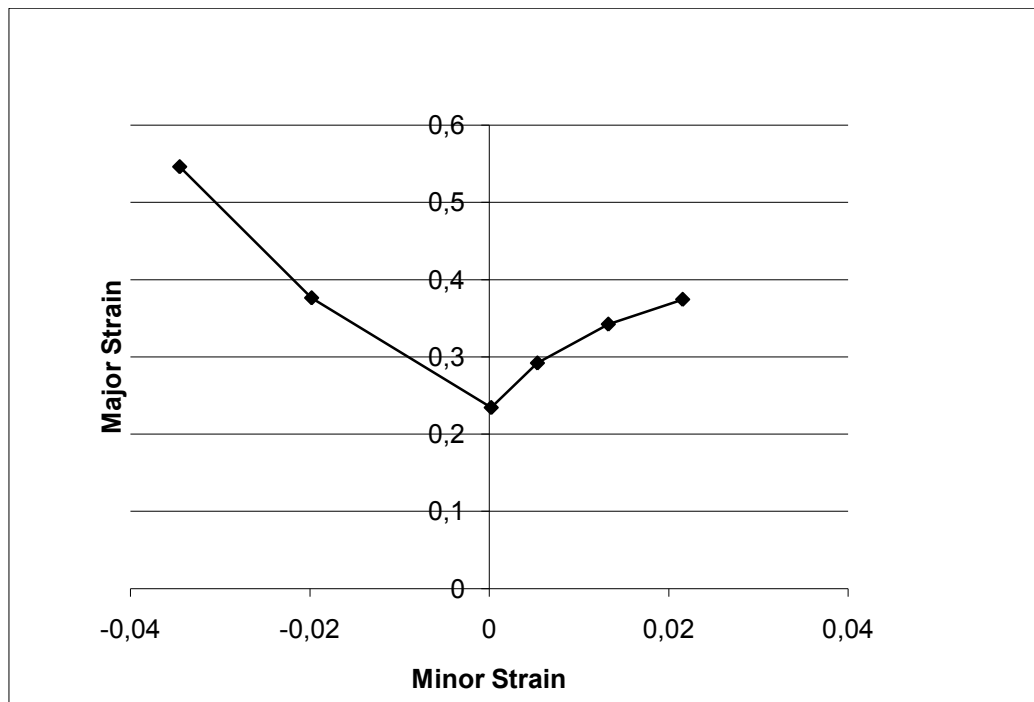
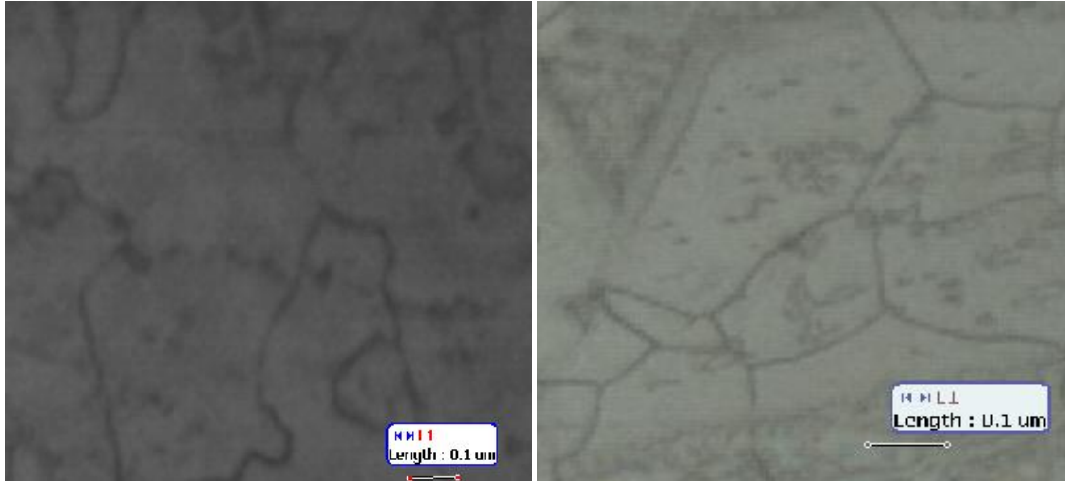


**Figure 5.2:** Forming limit diagram of the cold rolled St4 sheet

## 5.2 Microstructural Examination

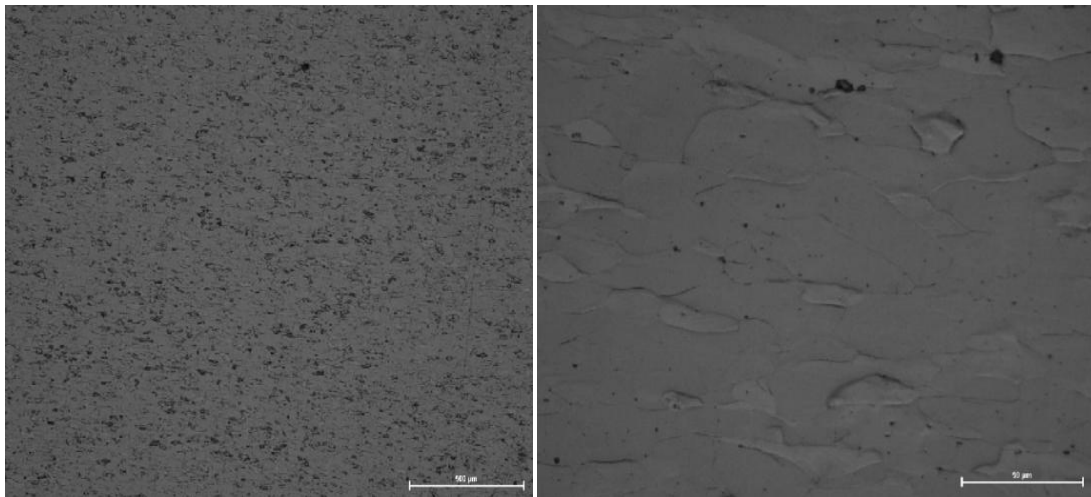
Before metallographic investigation for each specimen was finely ground, polished, and then, etched in %2 Nital.



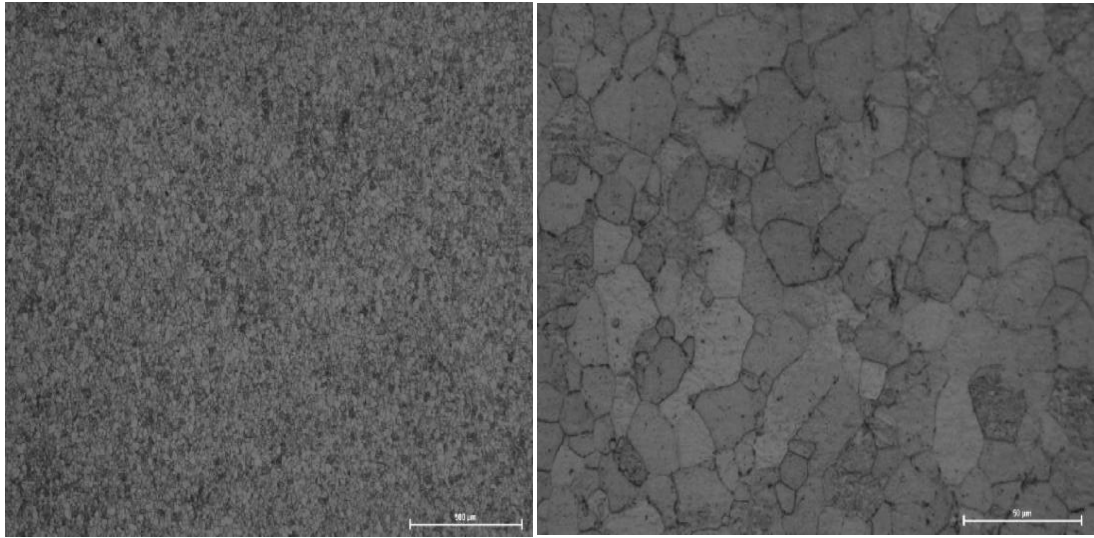
a)

b)

**Figure 5.3:** Micrographs representing the initial microstructure of St4 steel. a) 1.8mm thickness b) 1mm thickness



a)



b)

**Figure 5.4:** Micrographs representing the final microstructure of St4 steel. a) Bulged sample b) Deep drawn sample

As seen in Figure 5.3, initial microstructure of the cold rolled St4 sample consisted of ferrite phase, oxide impurities and grains.

The microstructure did not change during bulging deformation processes, still consisted of ferrite phases and oxide impurities. Therefore, one cannot expect any change in magnetic Barkhausen noise signals due to microstructural difference.

In the deep drawing microstructure one can see the elongated grains which were occurred by forming process.

### 5.3 Hardness Measurements

Hardness measurements on the initial samples gave the values in the 128-95 HB range. The highest and the lowest values were found near edge region. At the center, approximately 120 HB was obtained. The variations in the hardness results were caused by machining operations during sample preparation.

The final bulging samples hardness values were in the 131-124 HB range. There was a homogeneous distribution. At the center highest hardness value was obtained, 131 BH, near the edges the hardness value was 124 HB. The small differences in hardness values may come from deformation nature of the bulging operation. However, this small difference should not affect the magnetic Barkhausen noise measurements severely.

The final deep drawing samples hardness values were in the 148-138 HB range. Along the circumferential direction there was homogeneous distribution, 148-142 HB. In the axial direction, the hardness values were differentiated slightly. At the top and the bottom 138 HB value was measured, at the center 148 HB value was obtained.

#### **5.4 Measurements by Magnetic Barkhausen Noise Method**

The measurement method and the calibration process were explained in the previous section. Figure 5.5 shows the calibration curve between MBN and elastic tensile stress values. The relationship was formulated as:

$$\text{MBN signal amplitude} = 0.2058 \sigma + 158.92 \quad (5.1)$$

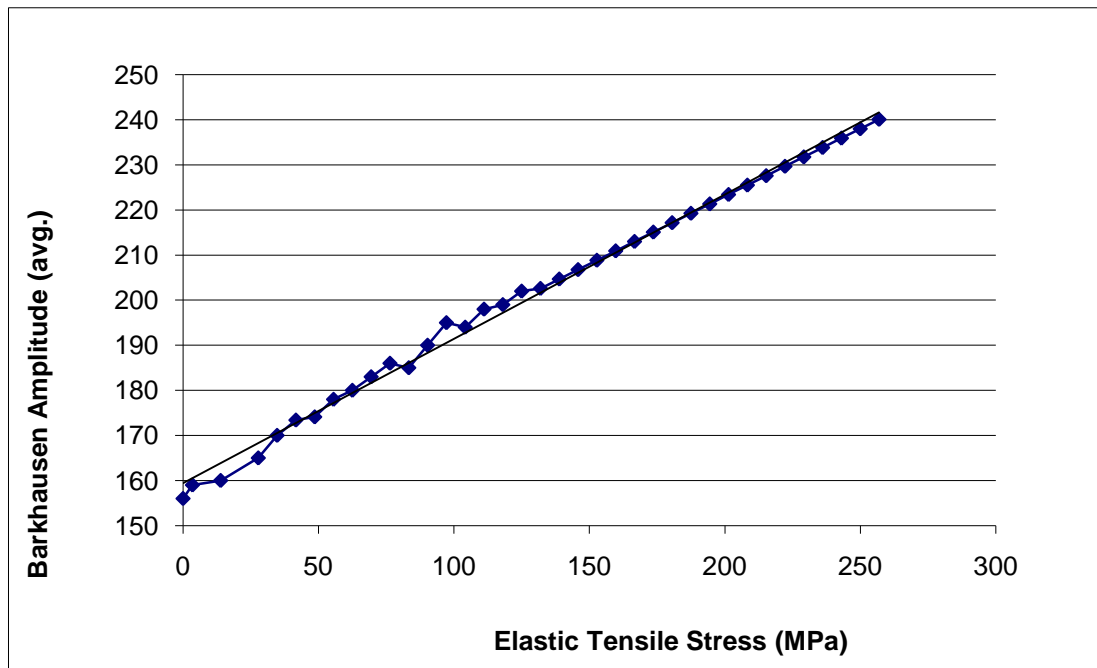


**Figure 5.5:** Calibration curve for MBN signal versus elastic tensile stress

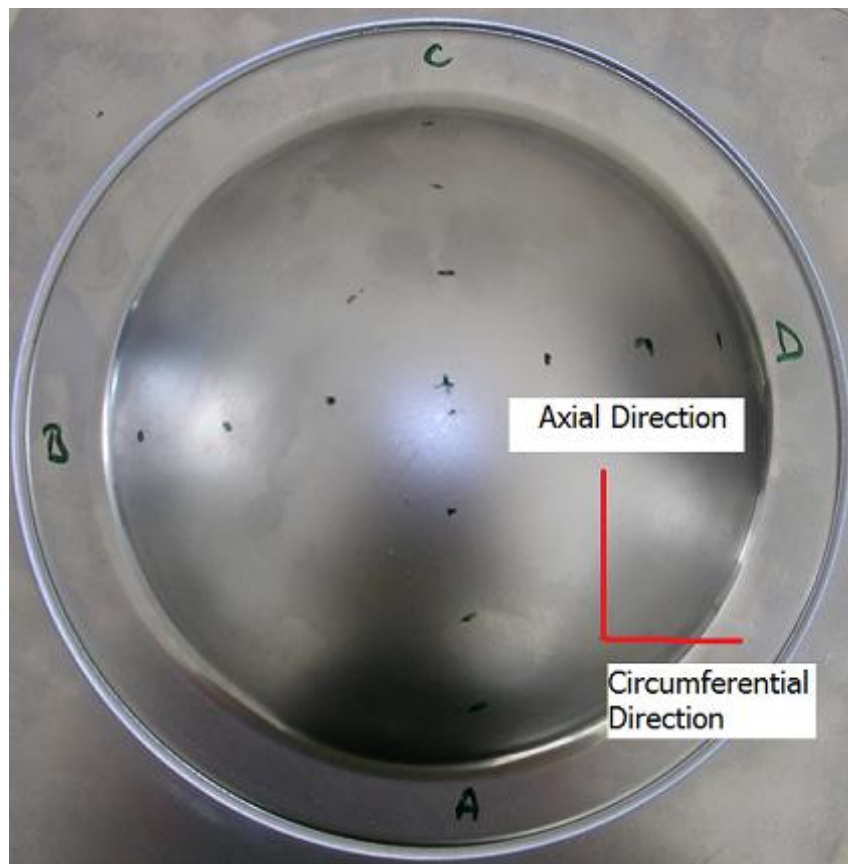


**Figure 5.6:** Representation of measurement directions on the bulged sample

### 5.4.1 Rollscan Results

Rollscan is a digital Barkhausen noise analyzer. It uses 125 Hz magnetization frequency. The magnetization and the amplification parameters which are the most effective parameters on MBN responses were used as 10 and 50, respectively.

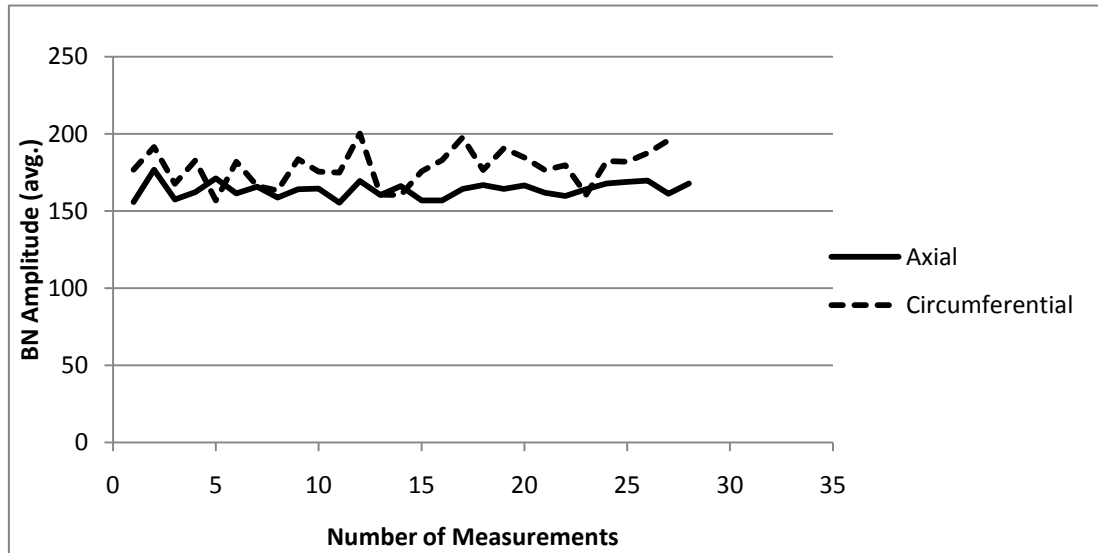
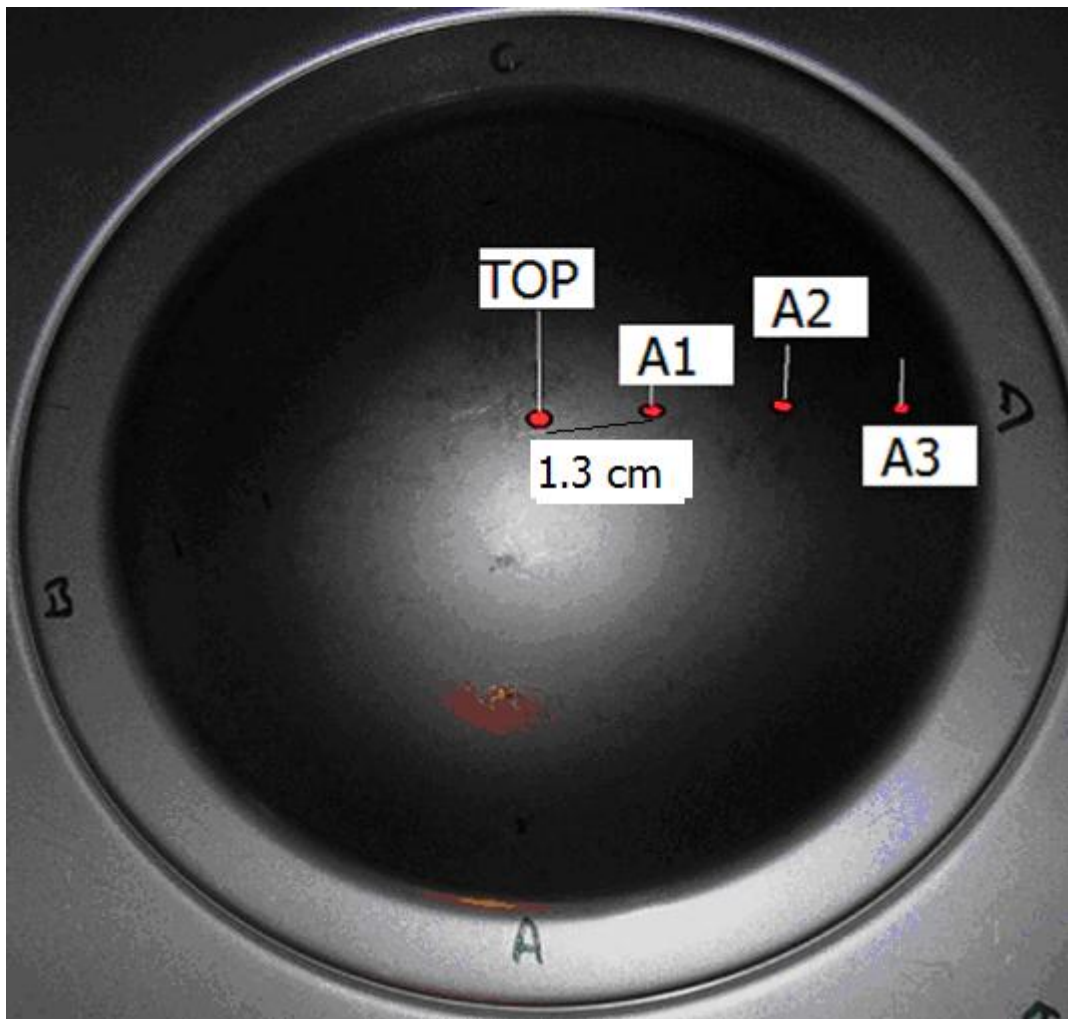


**Figure 5.7:** Surface residual stresses in the unprocessed sample, determined by MBN measurements.

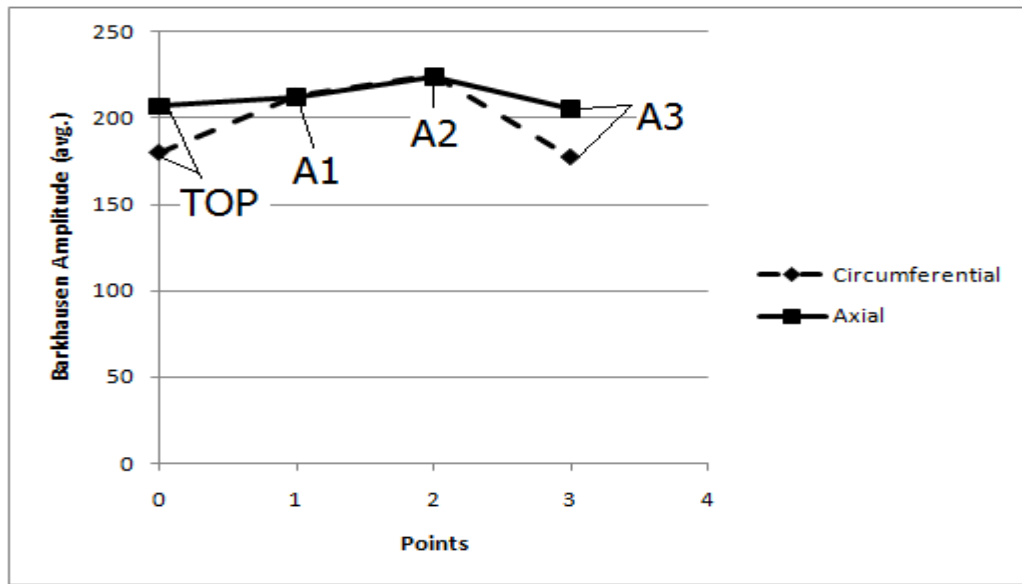
At the initial condition, residual stress distribution in the sample was nearly homogenous; i.e., about 191 MPa in axial and 188 MPa in circumferential directions.

### 5.4.2 $\mu$ Scan Results

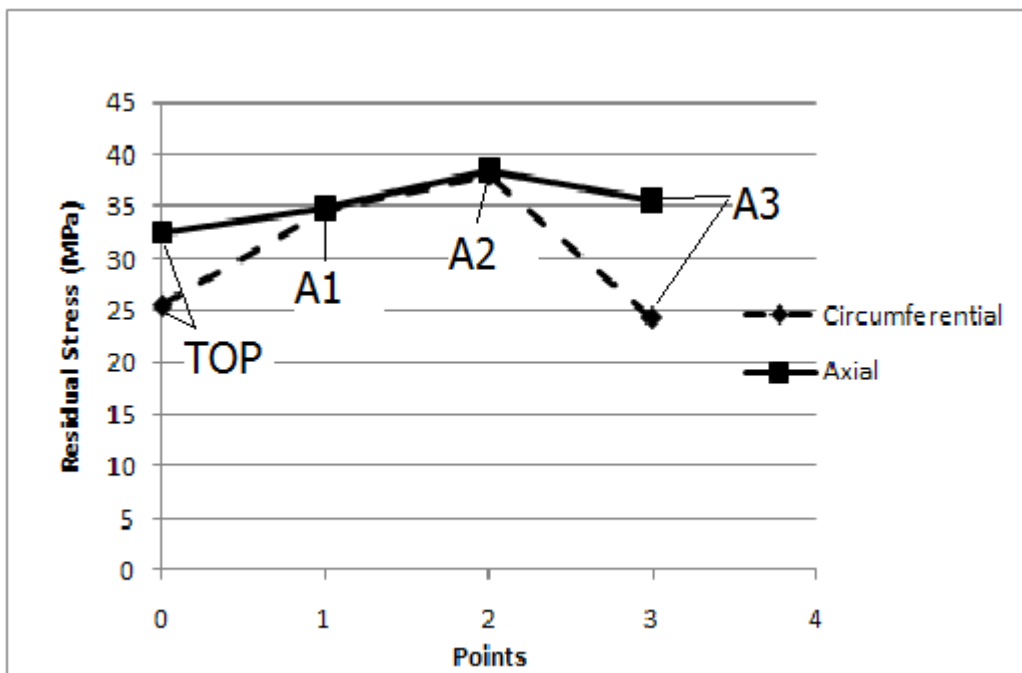
RMS (Root Mean Square) of magnetic Barkhausen noise was given by  $\mu$ scan channel analyses the raw MBN signal by Fast Fourier Transformation, and gives various graphs such as MBN fingerprint, amplitude vs. frequency graph, local hysteresis curve, etc.



**Figure 5.8:** The top and side views of the bulged sample. Measurements were taken from dotted points, A1, A2, A3 and TOP, in the circumferential and axial directions; there is 1.3 cm between the points.



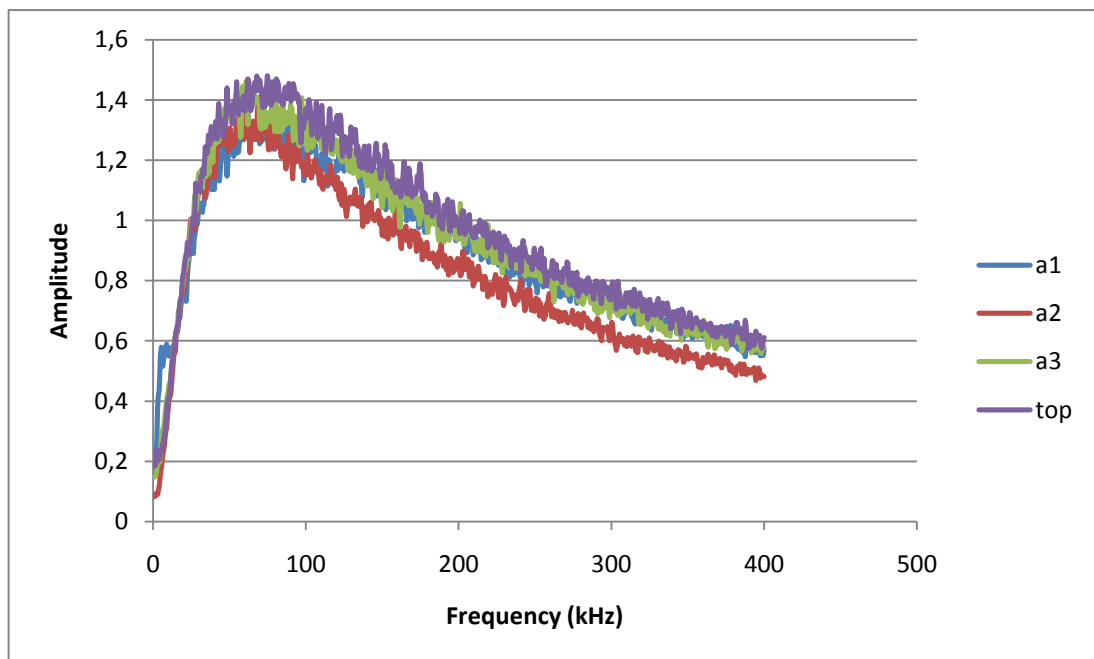
**Figure 5.9:** Surface magnetic Barkhausen noise values at the selected points of the bulged sample. Measurements were taken from dotted points, A1, A2, A3 and TOP; there is 1.3 cm between the points.



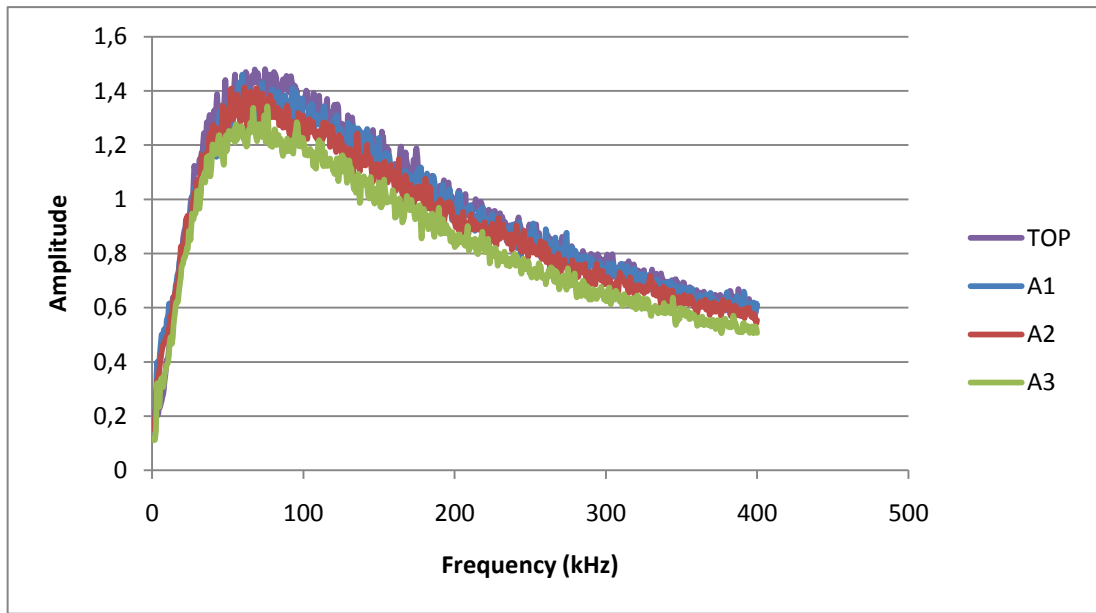
**Figure 5.10:** Surface residual stresses at the selected points of the bulged sample. Measurements were taken from dotted points, A1, A2, A3 and TOP; there is 1.3 cm between the points.

Figure 5.11 and 5.12 show that the amplitude frequency distribution figures were nearly same for all points and directions. Figure 5.13 and 5.14 show the MBN fingerprint (RMS profiles) of the bulged sample in two directions. The bulged sample has tensile residual stress according to these curves. The maximum value was seen at the top but the other points are not very different. Figure 5.15 and 5.16 show the local hysteresis curves. The highest flux was determined at the top point for both of the directions.

Tensile residual stress provides easy domain wall motion, so the MBN signals can reach higher amplitudes. The results showed nearly same profile as circumferential in the axial direction. During bulging operation biaxial pressure applied on the surface and the results was in the same approach.



**Figure 5.11:** MBN frequency distribution at the selected points on the bulged sample in the circumferential direction. Measurements were taken from dotted points, A1, A2, A3 and TOP; there is 1.3 cm between the points.



**Figure 5.12:** MBN frequency distribution at the selected points on the bulged sample in the axial direction. Measurements were taken from dotted points, A1, A2, A3 and TOP; there is 1.3 cm between the points.

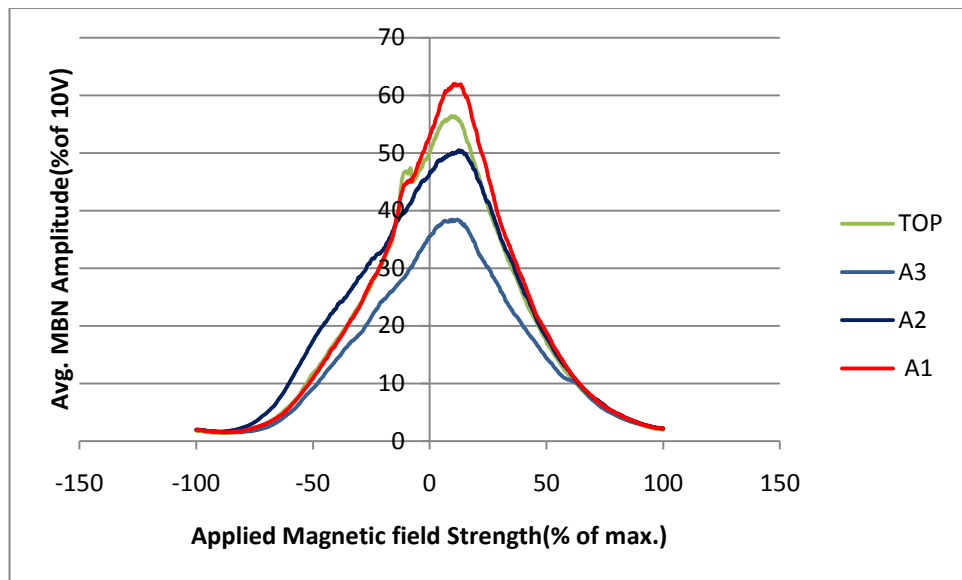


**Figure 5.13:** MBN fingerprint curves at the selected points on the bulged sample in the circumferential direction. Measurements were taken from dotted points, A1, A2, A3 and TOP; there is 1.3 cm between the points.

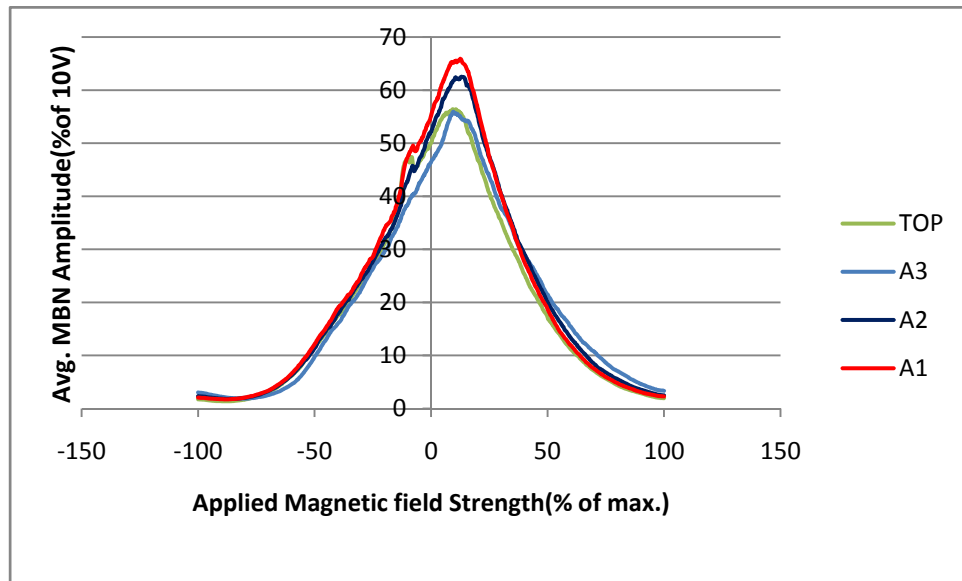


**Figure 5.14:** MBN fingerprint curves at the selected points on the bulged sample in the axial direction. Measurements were taken from dotted points, A1, A2, A3 and TOP; there is 1.3 cm between the points.

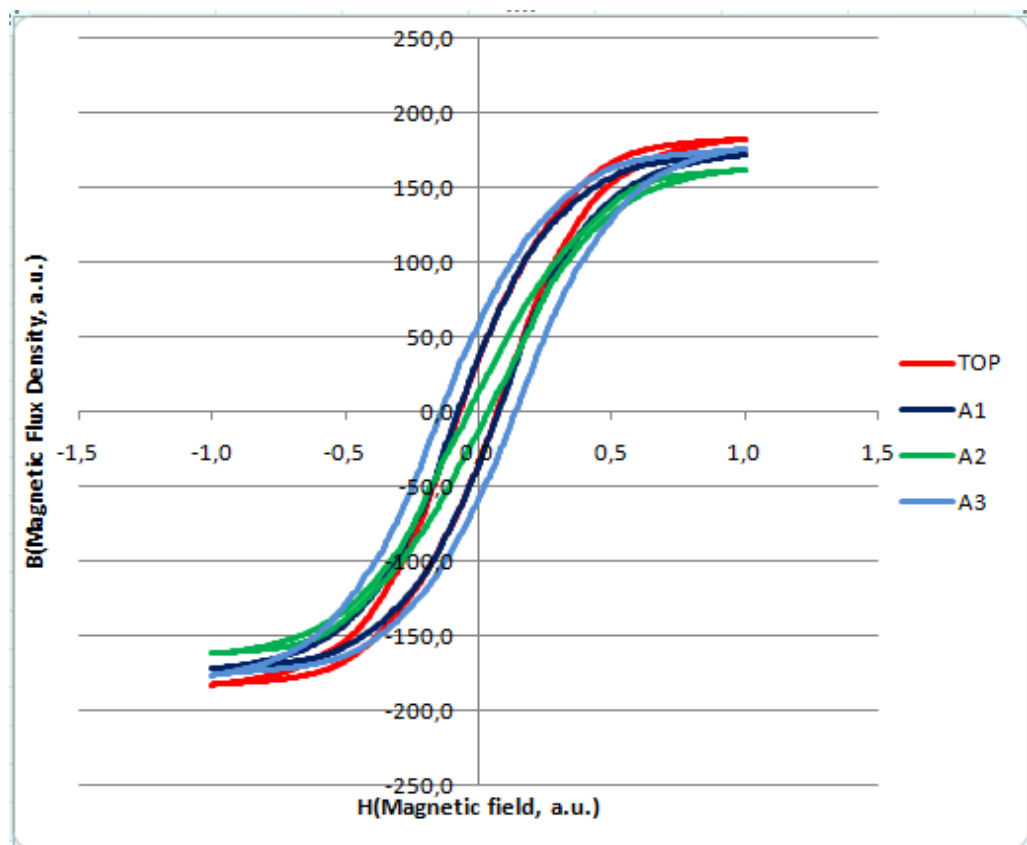


**Figure 5.15:** Hysteresis curves at the selected points on the bulged sample in rolling direction. Measurements were taken from dotted points, A1, A2, A3 and TOP; there is 1.3 cm between the points.

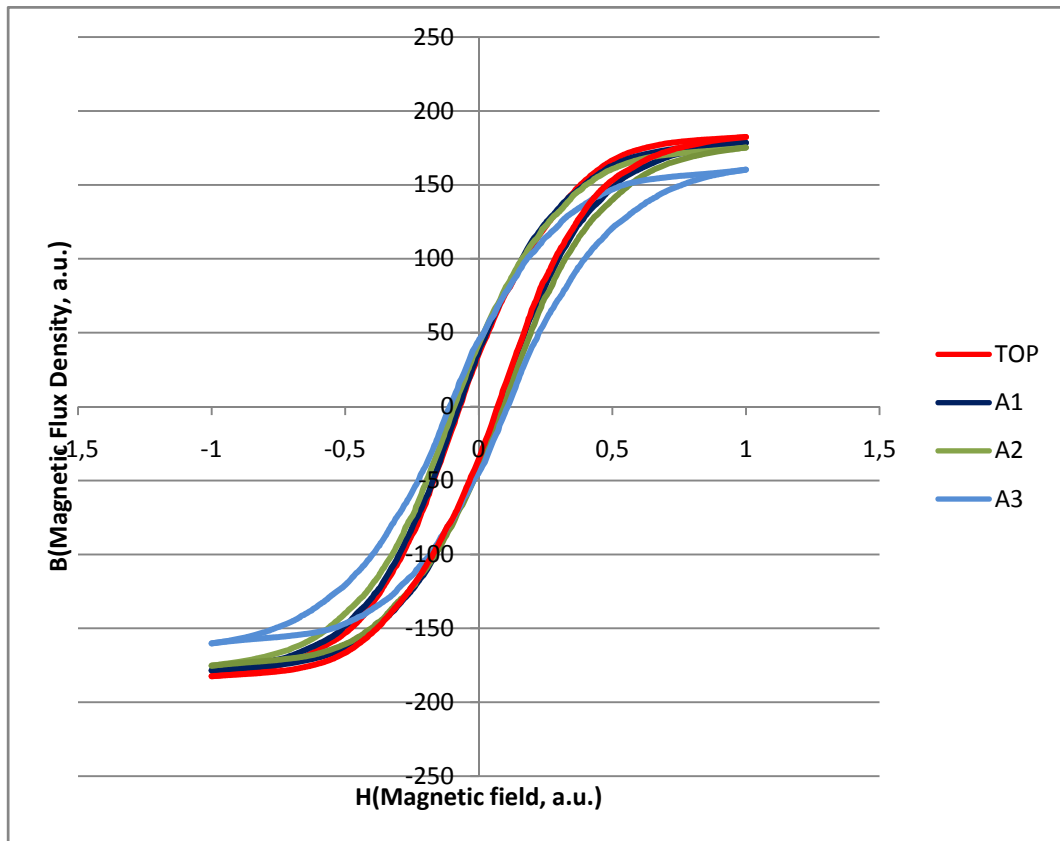


**Figure 5.16:** Hysteresis curves at the selected points on the bulged sample in axial direction. Measurements were taken from dotted points, A1, A2, A3 and TOP; there is 1.3 cm between the points.

## 5.5 Measurements by X-Ray Diffraction Method



**Figure 5.17:** Deep Drawing stages and the final sample

Surface residual stresses in the deep drawn samples were measured by X-ray diffraction method. Five samples were measured along their widths. Center of Gravity and Parabola Fit methods were used to calculate residual stress. Since both methods give almost the same results, only the results obtained by the Parabola Fit method were given. Elastic modulus was taken as 212 GPa; Poisson's ratio as 0.3. The (211) plane was selected as the reference peak with a diffraction angle of  $156.8^\circ$  at the stress-free state.

X-ray diffraction results were verified by taking two measurements at the same point. The values were nearly same for each measurement, residual stress state around 30 MPa in circumferential and -50 MPa in axial directions. Repeatability measurement results, analyzed by Center of Gravity method, are given in Figure 5.19.

As seen in Figure 5.20, the surface residual stresses are tensile in the circumferential direction and compressive in the axial direction. At the edges these values showed differences, trimming and bending operations may be the cause of this. Maximum residual stress exists at the center of the deep-drawn housings.

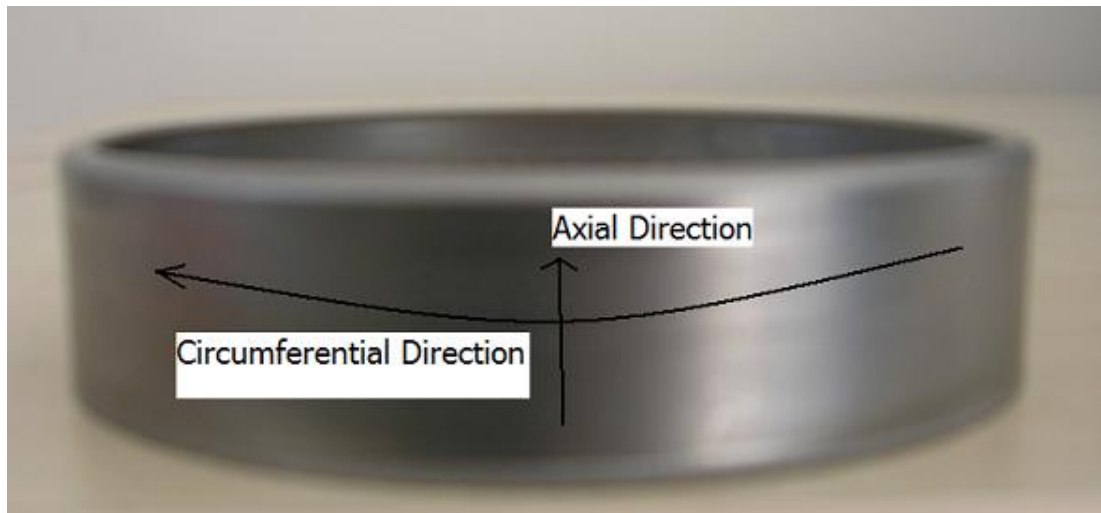


**Figure 5.18:** X-ray diffraction method measurement directions on deep drawn sample

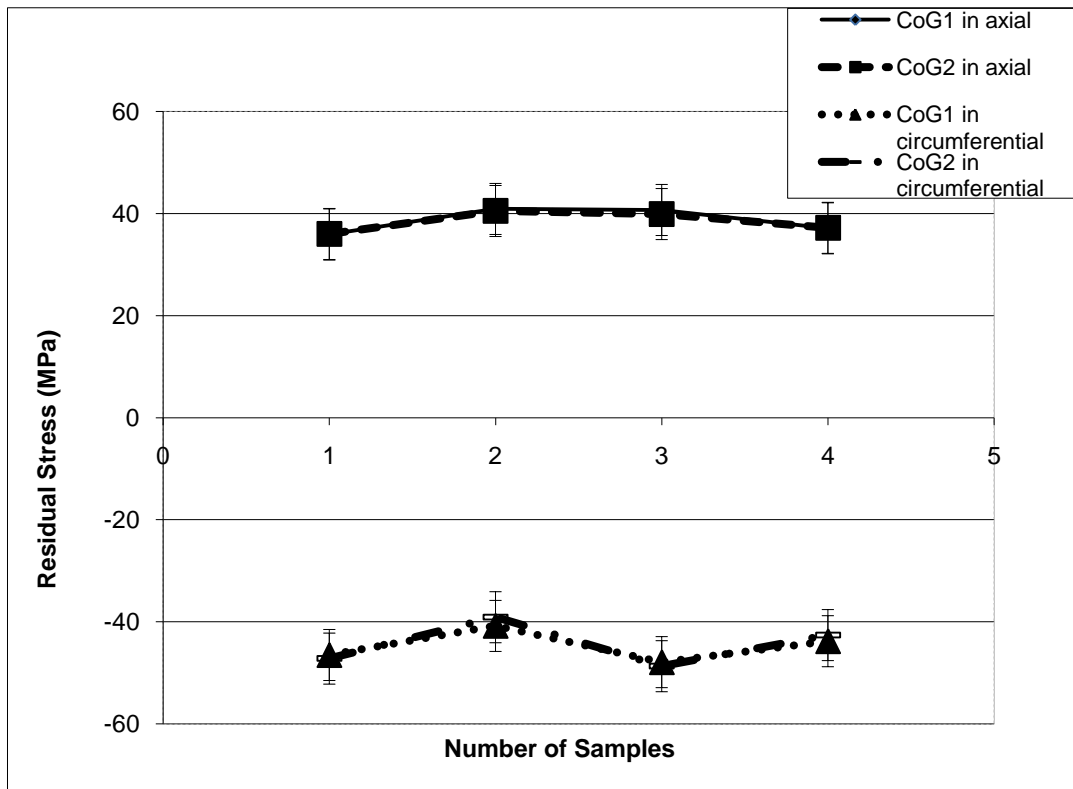


**Figure 5.19:** Repeatability measurements in the circumferential and axial directions by Center of Gravity method

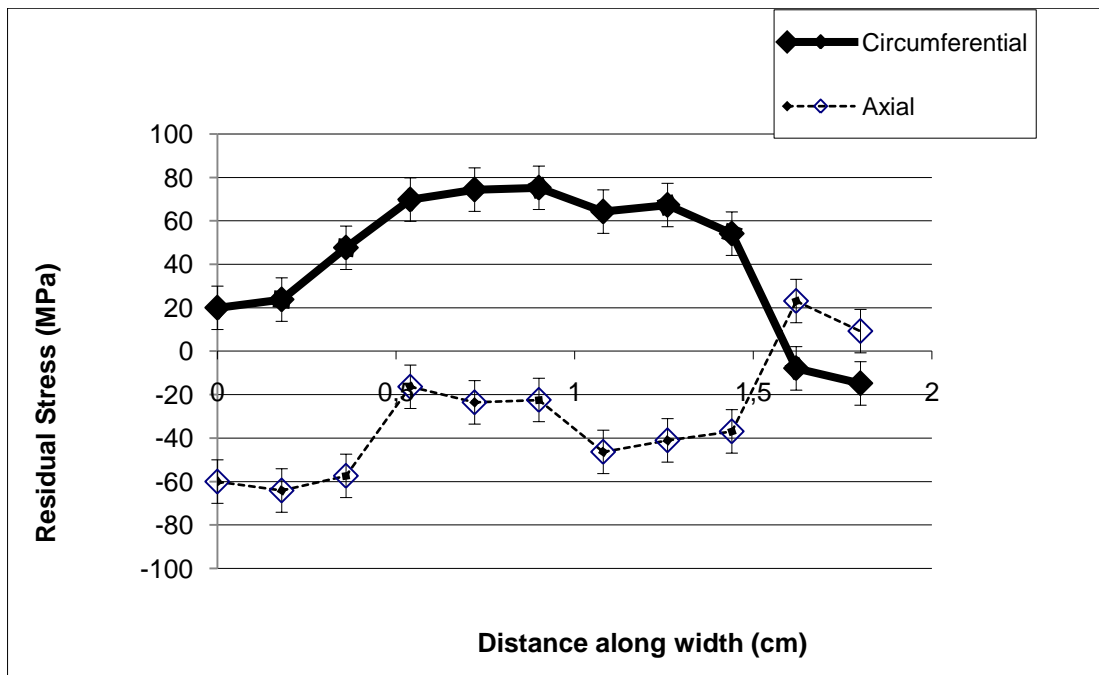


**Figure 5.20:** Surface residual stresses on the deep drawn sample, in the axial and circumferential directions.

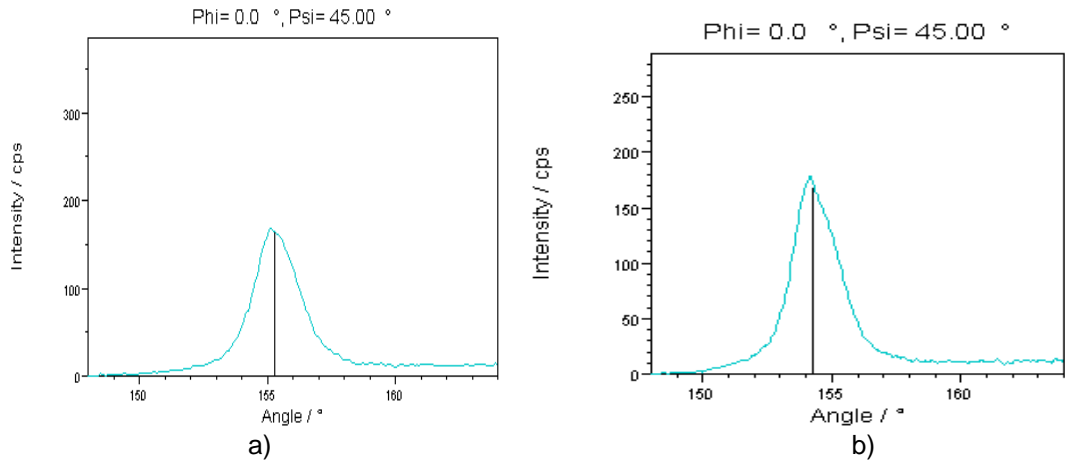


**Figure 5.21:** X-ray diffraction peaks. a) Compressive residual stress state diffraction peak. b) Tensile residual stress state diffraction peak.

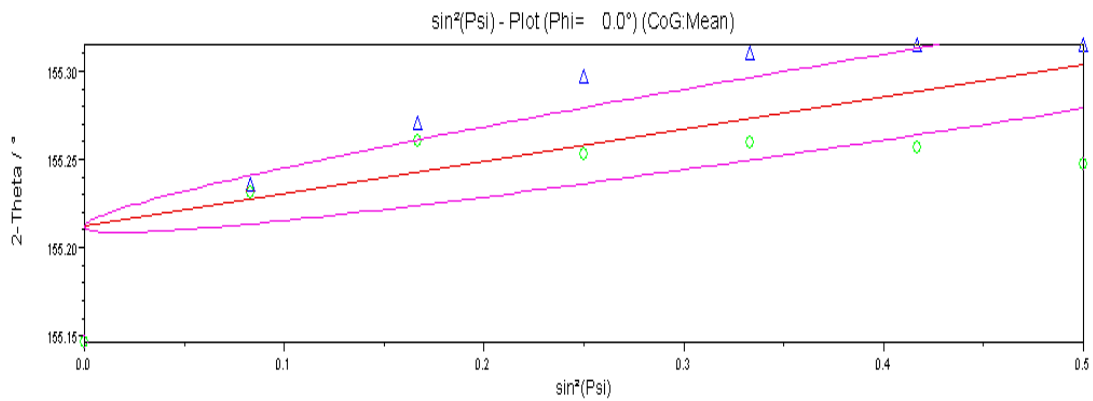


**Figure 5.22:** 2-Theta vs.  $\sin^2(\Psi)$  peak from measurements

## 5.6 Finite Element Simulations

After deformation process the deformed sample residual stress state was obtained from the reference information, because initial sample was assumed as residual stress free in simulation operations.

Bulging simulation was performed with MSC-Marc and deep drawing simulation was performed with Simufact.forming.

### 5.6.1 Bulging Simulation

In this simulation St4 cold rolled steel's mechanical properties implanted according to material characterization tests. Boundary conditions were described according to experimental pressure versus time data from hydraulic bulge test. Bulge simulation material parameters were described in Table 5.1.

**Table 5.1** Simulation Parameters

Elastic Modulus	212 GPa
Poissons Ratio	0.3
Material Model	Elasto-plastic
Hardening Model	Isotropic Hardening
Yield Criteria	Von- Misses
Material Mechanic Property	Isotropic
Element Type	8-nodes Quadrilateral
Flow curve	Ludwig ( $\sigma=K\varepsilon^n$ )

The simulation results were around 30MPa and tensile (Figures 5.23 and 5.24), by assuming the initial sample without any residual stress, and were correlated with experimental results. The residual stress state was same for rolling and axial directions, as expected. These results were “qualitatively” same as magnetic Barkhausen noise results.

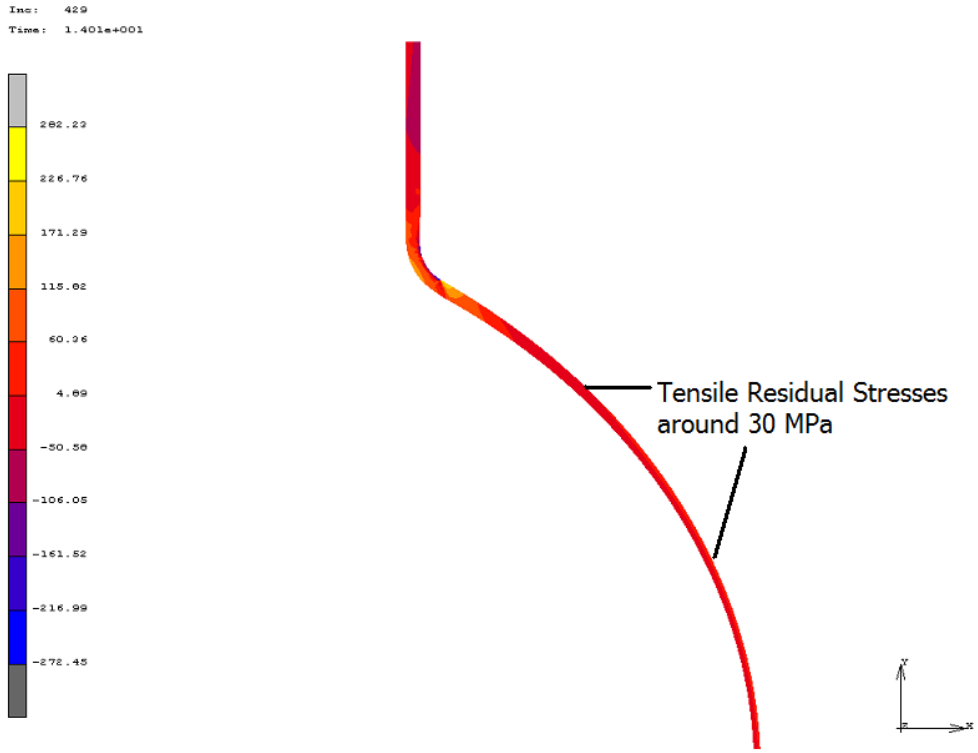


**Figure 5.23:** Tensile residual stress distributions in circumferential direction

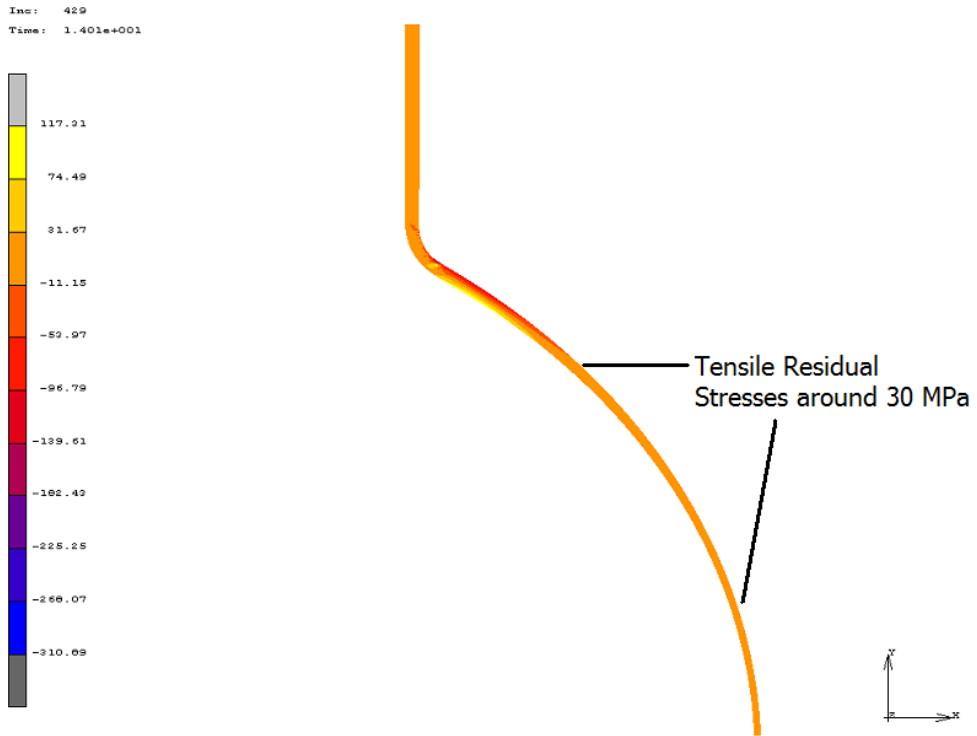


**Figure 5.24:** Tensile residual stress distributions in axial direction

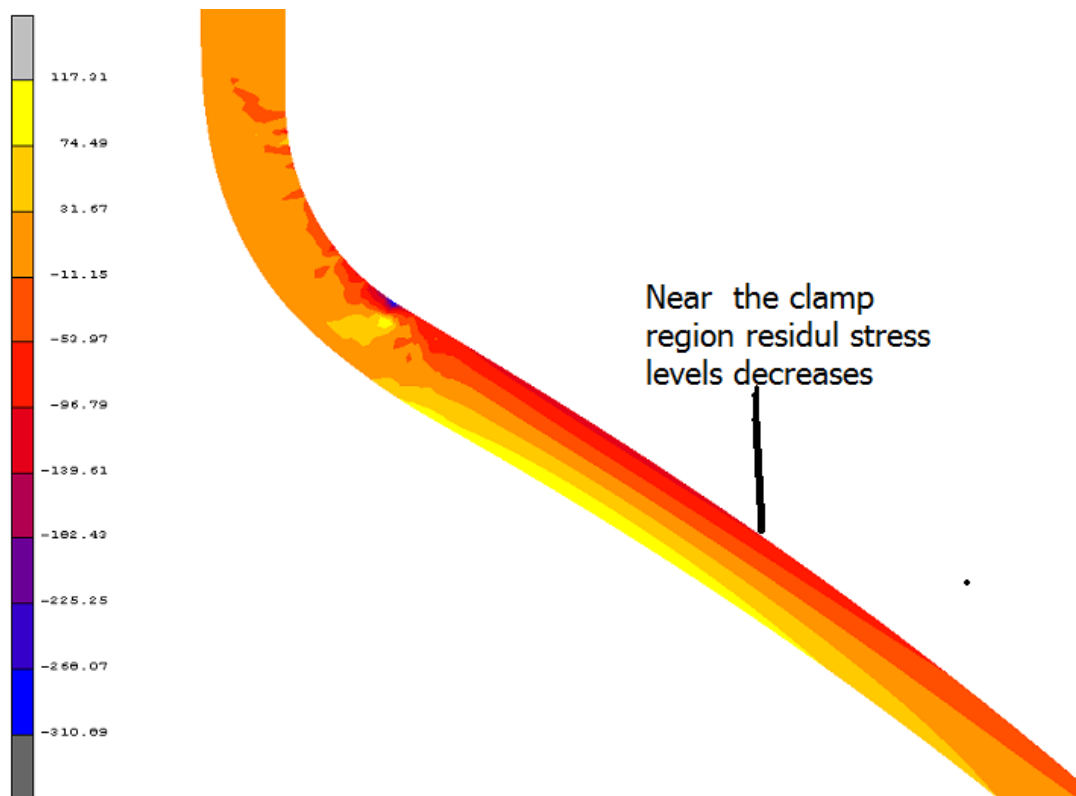


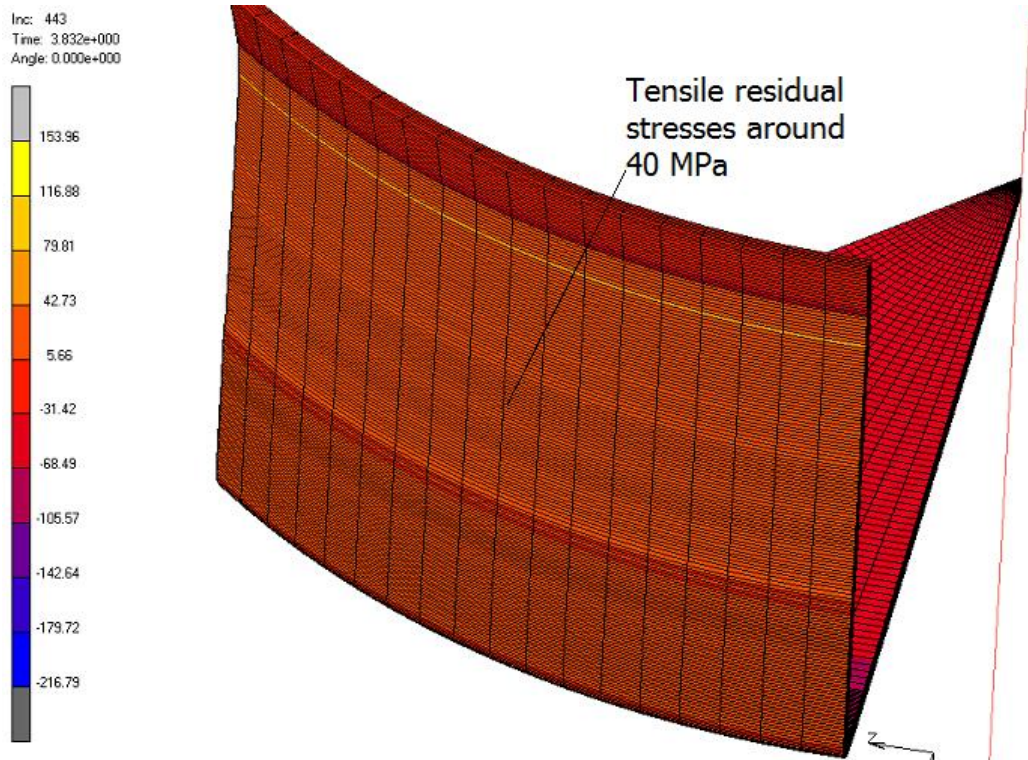
**Figure 5.25:** Residual stress level near clamp region

### 5.6.2 Deep Drawing Simulation

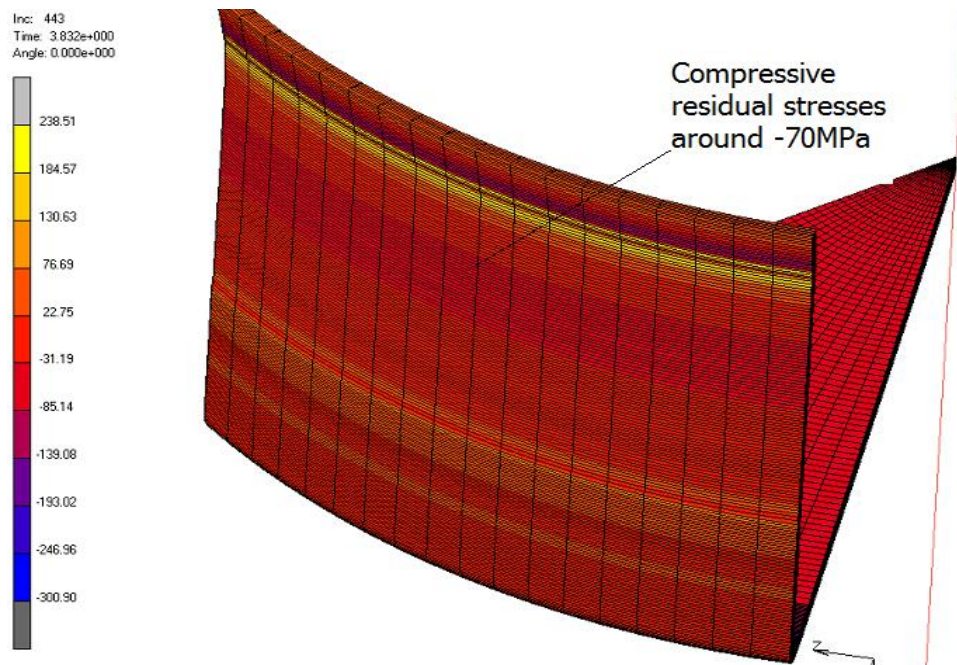
This analyze was done by Simufact.forming software program. Material parameters were described in Table 5.1.

Figure 5.25 shows the residual stress distribution in circumferential direction. The results were around 40 MPa, at the top and the bottom there was differences in residual stress values. This may cause of trimming and clamping operations. In deep drawn operation, the residual stress state expected to be tensile in circumferential direction and compressive in axial direction. Simulation results attest this.

Figure 5.26 shows the residual stress distribution in circumferential direction. The results were around -70 MPa. The same differences due to trimming and clamping operations were shown in these results.



**Figure 5.26:** Tensile residual stress distributions in circumferential direction



**Figure 5.27:** Compressive residual stress distributions in axial direction

Simufact.forming output data was shown by the graph in figure 5.27. The maximum and the minimum residual stress values were seen in the middle of the width. In the former studies, the authors also concluded the same results [40].

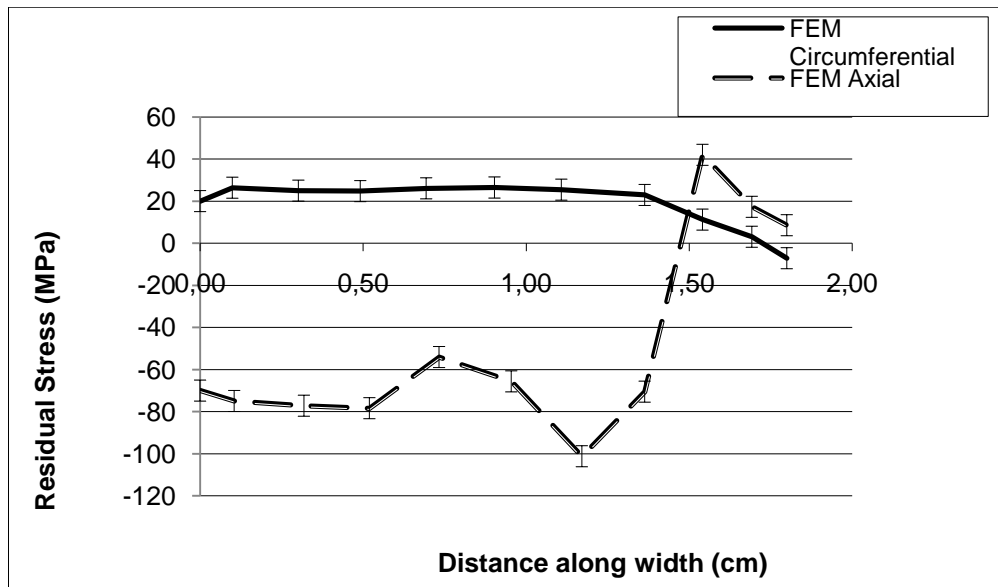
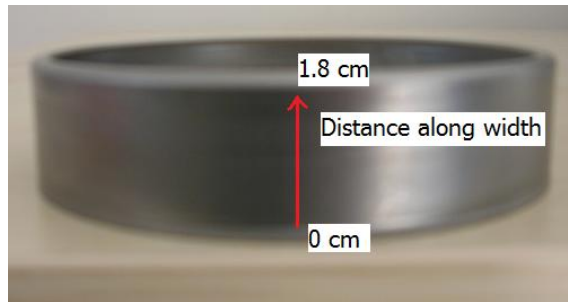


**Figure 5.28:** Simulation results: Residual stress distributions along the sample width in axial and circumferential direction

## 5.7 Discussion

Except some points, experimental and numerical results were correlated with each other. This may have a lot of different causes:

- Assuming elastic modulus as isotropic;

- Having curvature effect;
- Measurement mistakes;
- Rolling direction assumptions;
- Bulk modulus assumptions;
- Having texture.

### 5.7.1 Residual Stress State after Bulging

The simulation results were around 30 MPa, but there was a high increase in near edge region due to clamping. In the edge region residual stress value exceeded 200 MPa. The bulging operation provides biaxial stress state on the sample, so one can assume that the axial and circumferential residual stress levels will be same for the same regions. The experimental and numerical measurements gave the expected results.

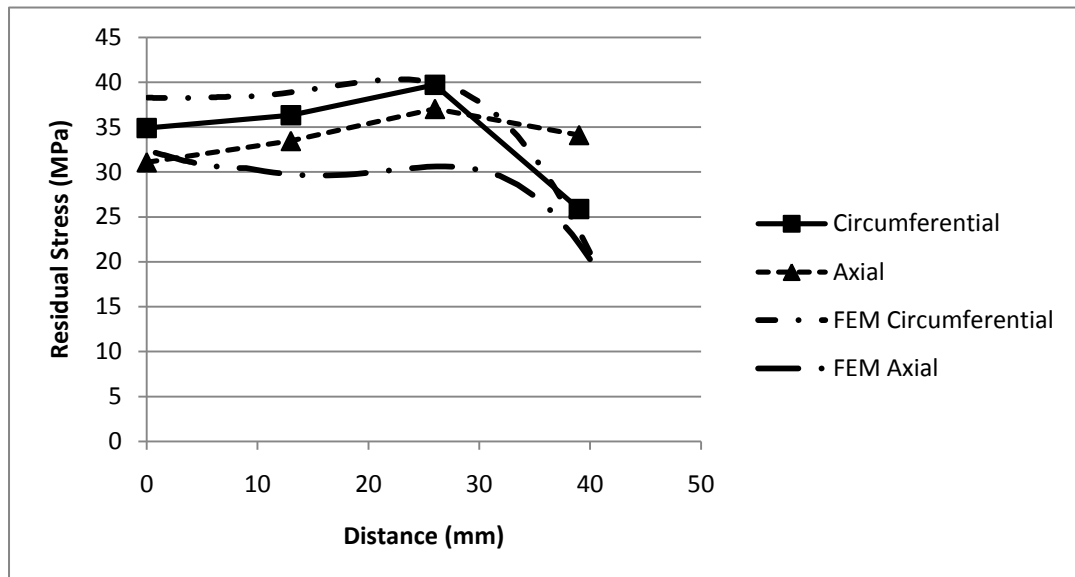


**Figure 5.29:** Comparison of residual stresses obtained by simulation and MBN measurements

### 5.7.2 Residual Stress State after Deep Drawing

The figure 5.24 summarizes the relation between X-ray diffraction measurements and Simufact.forming analyzes results. The exact values were not same but qualitatively both of them gave the same figure for axial and circumferential directions. So one can say that finite element simulations give nearly same result as experimental values for residual stress state of deep drawn steel sheets.

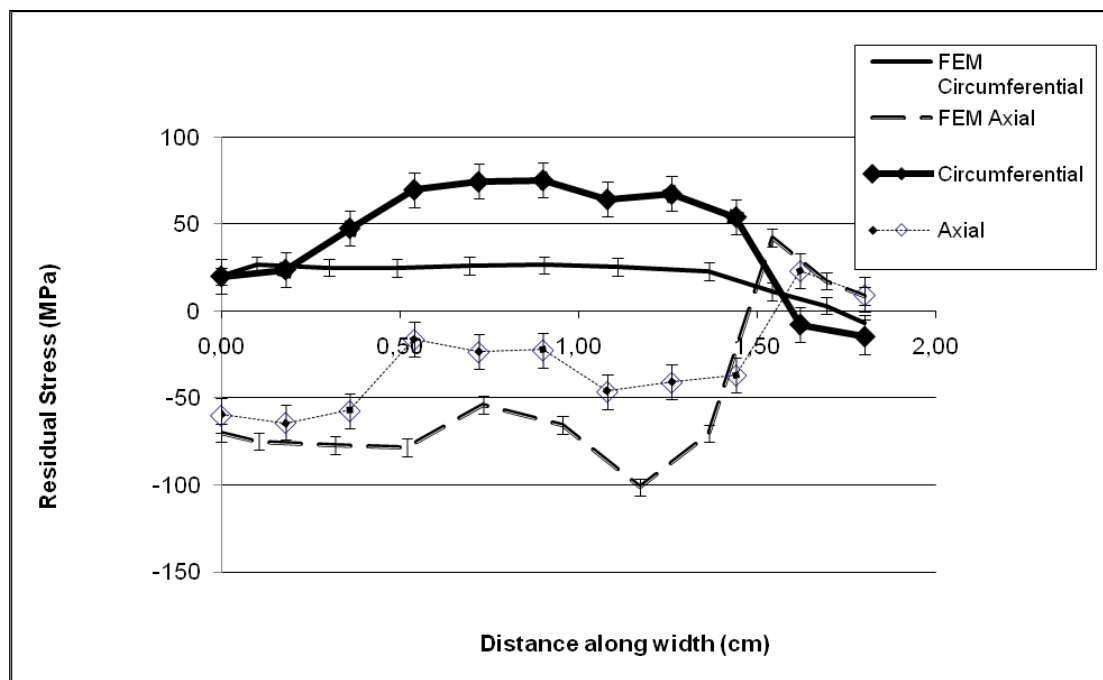


**Figure 5.30:** Comparison of simulation (FEM) and X-ray diffraction measurement results in axial and circumferential directions

### 5.7.3 Dimensional Correlation

Dimensional comparison was also made for bulged and deep drawn samples. The simulated and experimental processes gave nearly same values. The maximum error was seen in bulged sample thickness values, 5.08 %. These values can be directly measured, residual stress states were measured indirectly; i.e. from strain values, so

dimensional correlation is very exact verifying the relation between experimental and simulation processes.

**Table 5.2** Bulging Operation Dimensional Correlation

	Simulation	Experimental	$\Delta$ %
Dome Height	43.8818 mm	43.35 mm	1.21 %
Thickness	0.8308 mm	0.873 mm	5.08 %

**Table 5.3** Deep Drawing Operation Dimensional Correlation

	Simulation	Experimental	$\Delta$ %
Height	23.89mm	23.62mm	1.13 %
Thickness	0.8641mm	0.9mm	4.15 %

## CHAPTER 6

### CONCLUSIONS

In this study, numerical and various experimental methods were used in order to determine the surface residual stresses in the sheet samples deformed by hydrostatic bulge test and deep drawing. The samples were prepared from the cold-rolled St4 steel sheets.

As the initial step, several mechanical tests were performed in order to supply the input data to the computer simulations via MSC.MARC and Simufact-forming software.

For the measurement of the surface residual stresses, X-ray diffraction method was used for the deep drawn samples, and Magnetic Barkhausen Noise method was used for the samples deformed by hydrostatic bulge test. Finally, numerical and experimental results were discussed and compared.

The following points can be concluded from the outputs of the thesis work.

- Deep drawing operation introduces tensile residual stresses in the circumferential direction and compressive residual stresses on the axial direction of the sample.
- Bulging operation introduces tensile residual stress in both of the circumferential and axial directions since biaxial force was applied on the specimen.

- Simulation results are in agreement with the experimental results. FEM is very beneficial to determine the residual stress state in the deformed sheet samples. However, obtaining correct material input data via carefully performed tests is a critical issue in order to get reliable results.
- X-ray diffraction technique successfully measures the residual stresses in the deep drawn sheets.
- Magnetic Barkhausen Noise technique is a fast and effective method to measure the surface residual stresses. In a very short time it is possible to obtain the residual stress map of the surface of the deformed sheet. However, it requires a very careful calibration on a reference sample, and any change in the microstructure may decrease the reliability of the stress measurements.

These studies can be repeated for high carbon or alloy steels, also for the components having more complex geometries.

## REFERENCES

- [1] Dieter G.E., *Mechanical Metallurgy*, McGraw-Hill, 2001, p.666
- [2] Wikipedia, [http://en.wikipedia.org/wiki/Deep\\_drawing](http://en.wikipedia.org/wiki/Deep_drawing), last visited on 09.10.2010
- [3] Medraj M., Mechanical Engineer Department. Concordia University Lecture Notes, 2008
- [4] Olsson D.D., Bay N., Andreasen J.L., *Lubricant test for punching and blanking*. Advanced Technology of Plasticity. Proc. 7th ICTP, Yokohama, 2002, p.757-762.
- [5] Danckert J., *Reduction of the Residual Stresses in a Deep-Drawn Cup by Modifying the Draw Die Profile*, Aalborg University, January 1995
- [6] Marciniak, Z., Duncan, J.L., Hu, S. J., *Mechanics of Sheet Metal Forming*, 2<sup>nd</sup> Edition, Butterworth-Heinemann, Oxford, 2002.
- [7] Custompartnet, <http://www.custompartnet.com>, last visited on 15.11.2010
- [8] *Metal Forming Handbook*, Schuler, Springer-Verlag, Berlin Heidelberg, 1998, p. 156- 193
- [9] Kakandikar G.M., Nandedkar V.M., *Optimization of forming load and variables in deep drawing process for automotive cup using Genetic Algorithm*, IISc Centenary-International Conference on Advances in Mechanical Engineering IC-ICAME, Bangalore, 2008
- [10] Nastran M., Kuzman K., *Stabilizing the forming properties of wire by using a rollerstraightening process*, Journal of Mechanical Engineering, Vol. 49, Nr. 6, 2003, p.298-312
- [11] Altan T., *Forming lightweight alloys*, UHSS emphasis of study. June 12, 2007 78

- [12] Withers P. J., Bhadeshia H. K. D. H. *Residual stress part 1- measurement techniques*, Materials Science and Technology, Vol. 17, 2001, p. 355-365.
- [13] Finlayson T.R., *Residual stress analysis: a review*, Metals Forum, Vol. 6, No 1, 1983
- [14] European Network of Surface and Prestress Engineering and Design, <http://www-ensped.utt.fr/aboutprestress/definition.htm>, last visited on 21.08.2010
- [15] Residual Stress, <http://www.residualstress.org/>, last visited on 14.02.2010
- [16] Withers P. J., Bhadeshia H. K. D. H. *Residual stress part 2- nature and origins*, Materials Science and Technology, Vol. 17, 2001, p.366-375.
- [17] Handbook of residual stress and deformation of steel, ASM International, 2002, p.112-113
- [18]. Prev y P.S., *X-ray diffraction residual stress techniques*, Metals Handbook, Metals Park: ASM, 10 (1986) 380-392.
- [19] Columbia University, <http://ehs.columbia.edu/>, last visited on 03.10.2009
- [20] Ruud C.O., Farmer G. D., “*Residual stress measurement by x-rays: errors, limitations and applications*”, Nondestructive evaluation of materials, ed. By Burke J.J. and Weiss M., Plenum Press, 1979, p.101-116
- [21] Ruud C.O., *X-Ray Analysis and Advances in Portable Field Instrumentation*, J. Met, Vol31 (No:6 ), Jun 1979 , p.10-15
- [22] Willcox M., Mysa T., *An Introduction to Barkhausen Noise and its Application*, <http://www.insight-ndt.com/>, last visited on September 2010
- [23] Stewart D.M., Stevens K.J., Kaiser A.B., *Magnetic Barkhausen noise analysis of stress in steel*, Current Applied Science, 4 2-4, 2004, p.308-311

- [24] Tönshoff H.K., Friemuth T., Oberbeck I., Seegers H., *Micromagnetic Stress Determination on Tailored Blanks*, 15th World Conference on Nondestructive Testing Roma (Italy), 15-21 October 2000
- [25] Tiito K., in *Nondestructive Evaluation: Application to Materials Processing*, ed. By Buck O., Wolf S.M., ASM, Materials Park, Ohio, 1984, p. 161
- [26] Durin G., Zapperi S., "The Science of Hysteresis", vol. II, Bertotti G., Mayergoyz I. eds, Elsevier, Amsterdam, p.181-267, (2006)
- [27] Saquet O.,Chicois J., Vincent A., *Barkhausen noise from plain carbon steels: analysis of the influence of microstructure*, Materials Science and Engineering A,269 (1999), p.73–82
- [28] Jeong H. T., Park D. G, Hong J. H., Ahn S., Kim G.M., *The effect of microstructural changes on magnetic Barkhausen noise in Mn-Mo-Ni pressure vessel steel*,Journal of the Korean Physical Society, Vol. 34, No. 5, May 1999, p. 429-433
- [29] Gardner C. G., *Barkhausen noise analysis*, Proc. of a workshop on nondestructive evolution of residual stress, NTIAC-76-2 ,1975, p.211-217
- [30] Sundström O., Törrönen K., *The use of Barkhausen noise analysis in nondestructive testing*, Materials evaluation, February 1979, p.51-56
- [31] Ruud O. C., *A review for nondestructive methods for residual stress measurement*, NDT International, 15 1, 1982, p.15-23
- [32] M. Tisza, *Numerical Modeling and Simulation in Sheet Metal Forming Academic and Industrial Perspectives*, Materials Science Forum, 473-474 (2005) 135-140

- [33] Tekkaya, A. E., *State-of-the-Art of Simulation of Sheet Metal Forming*, Journal of Materials Processing Technology, 103 (2000) 1, p. 15-23.
- [34] Incandela O., Tabourot L., Porret p., Balland P., Arrieux R., Ducher F., *Modelling and analysis of a deep-drawing operation: key factors for successful comparisons between experimental and simulated results*, Journal of Materials Processing Technology, 155-156, 2004, p.1105-1110
- [35] Kleiner M., Krux R., Homberg W., *Analysis of Residual Stresses in High-pressure Sheet Metal Forming*, CIRP Annals, Manufacturing Technology Volume 53, Issue 1, 2004, p. 211-214
- [36] Axinte C., Iordache M., *Determination of residual stresses within the formed part*, Fascicle of Management and Technological Engineering, Vol. VII (XVII), 2008
- [37] Axinte C., Iordache M., *Determination of residual stresses within the formed part*, Scripta Materialia, Volume52,2005, p. 305–309
- [38] ] Danckert J., *Reduction of the Residual Stresses in a Deep-Drawn Cup by Modifying the Draw Die Profile*, CIRP Annals, Manufacturing Technology Volume 44, Issue 1, 1995, p. 259-262
- [39] Överstam H., *The influence of bearing geometry on the residual stress state in cold drawn wire, analysed by the FEM*, Journal of Materials Processing Technology Volume 171, Issue 3, 1 February 2006, p. 446-450
- [40] Berrahmoune M.R., Berveiller S., Inal K., Patoor E., Simon C., Glez J.C, *Determination of residual stresses after tensile tests and deep drawing of unstable austenitic steel*, Materials Science Forum ,490 – 491, 2005, p.590-595

[41] Thomas J., Mohan J., Kendrish S., Fix R. M., *Advanced Techniques for the Measure of Microstructure and Residual Stress in Components Subject to Rolling Fatigue*, American Stress Technologies, 2009, SAE International

[42] Blaow M., Evans J.T, Shaw B., *Effect of deformation in bending on magnetic Barkhausen noise in low alloy steel*, Materials Science and Engineering A, 386 1-2, 2004, p.74-80

[43] Epp J., Hirsch T., de Souza Rosendo T., *Use of X-ray diffraction and micromagnetic methods for a complete characterization of residual stress states in manufactured parts*, Materials Science and Engineering Technology, 40 5-6 ,2009, p.339–486

[44] Material Data Base, <http://www.matbase.com/material/ferrous-metals/high-strain-steel/st-14/properties> , last visited on December 2009

[45] Zwick/Roell Product Information text, 2009

[46] Fracz W., Stachowicz F., Slota J., Spisák E. , Comparison of uniaxial and biaxial stress-strain relationship of sheet metal, IX. International workshop, Moscow, 2003, p.92-95.

[47] Slota J., Spisák E, determination of flow stress by the hydraulic bulge test, Metalurgija, Series 47,2008 , p.13-17

[48] Hill R., *A theory of the plastic bulging of a metal diaphragm by lateral pressure*, Philosophical Magazine, Series 7 41, 1950, p.1113–1142.

[49] Norwegian University of Science and Technology, <http://www.ntnu.edu/simlab/testing/bup>, last visited on 20.09.2010

[50] GOM Optical Measurement Techniques, [www.gom.com](http://www.gom.com), last visited on 12.05.2010

- [51] Min J., Lin J., Cao Y., Bao W. and Lu Z., *Effect of necking types of sheet metal on the left-hand side of forming limit diagram*, Journal of Materials Processing Technology, 210 8, 2010, p.1070-1075
- [52] Stranoa M., Colosimo B.M., *Logistic regression analysis for experimental determination of forming limit diagrams*, International Journal of Machine Tools & Manufacture 46, 2006, p. 673–682
- [53] User Manual of Seifert XRD 3003 PTS, 2009
- [54] Bob B. H, Two Dimensional X-Ray Diffraction, Willey, 2009
- [55] MSC.SuperFormUser's Guide, 2008
- [56] Marc® 2007 Volume A: Theory and User Information, 2007
- [57] Simufact.forming overview, User Guide, 2009